THIN-FILM MIXED-METAL MOLECULE-BASED MAGNETS BY CHEMICAL VAPOR DEPOSITION

by

Preston Kaj Erickson

A thesis submitted to the faculty of
The University of Utah
in partial fulfillment of the requirements for the degree of

Master of Science

Department of Materials Science and Engineering

University of Utah

December 2011

The University of Utah Graduate School

STATEMENT OF THESIS APPROVAL

The thesis of **Preston Kaj Erickson**

has been approved by the following supervisory committee members:

Joel S. Miller, Chair		**09/23/11** Date Approved
Ashutosh Tiwari, Member		**09/26/11** Date Approved
Michael Scarpulla, Member		**09/26/11** Date Approved

and by **Anil Virkar**, Chair of

the Department of **Materials Science and Engineering**

and by Charles A. Wight, Dean of The Graduate School.

ABSTRACT

A chemical vapor deposition method has been developed for the synthesis of both $Co[TCNE]_2$ thin-films and $V_xCo_{1-x}[TCNE]_2$ thin-films. Both materials have been previously synthesized by various solution methods. The $Co[TCNE]_2$ thin-films were characterized by infrared spectroscopy and magnetometer, and were determined to be identical in structure and magnetic behavior to the analogous solution-prepared samples.

$V_xCo_{1-x}[TCNE]_2$, when prepared from solution, showed a composition dependence of the magnetic properties as well as the infrared characteristics. Higher cobalt concentrations led to higher coercive fields with respect to $V[TCNE]_2$, which has a coercive field of ~7 Oe at 5 K. At a composition of $V_{0.3}Co_{0.7}[TCNE]_2$ the coercive field is ~270 Oe at 5 K. The thin-films of this material showed the same infrared characteristics, based on composition, as the solution-prepared compounds. There was, however, no increase in coercive field at any composition, with a maximum coercive field measured as 10 Oe for a composition of $V_{0.45}Co_{0.55}[TCNE]_2$.

Dedicated to my wife, Kristyn, and my son, Bryce, who have been my support and my sanity through it all.

TABLE OF CONTENTS

LIST OF FIGURES

LIST OF TABLES

SYMBOLS AND ABBREVIATIONS

T_c	critical temperature
H	applied field
H_{cr}	coercive field
Oe	Oersted
M	magnetization
M_r	remnant magnetization
M_s	saturation magnetization
TCNE	tetracyanoethylene
CVD	chemical vapor deposition
z	ionic charge
ν_{CN}	wavenumber of C≡N stretch
SCCM	standard cubic centimeters per minute
KBr	potassium bromide
IR	infrared spectroscopy
χ	magnetic susceptibility
T	temperature
θ	Weiss constant
C	Curie constant

g	Landé factor
S	total spin quantum number
C_{Co}	concentration of cobalt
m	slope
x	fraction of V in $V_xCo_{1-x}[TCNE]_2$
SEM	scanning electron microscope
EDS	energy dispersive x-ray spectroscopy

ACKNOWLEDGEMENTS

Thanks go to Dr. Joel S. Miller for supervising me in this project, for prodding and leading as needed, and for helping me develop a strong research and work ethic; Bretni Kennon, for getting me off to the right start; Amber McConnell and Jack DaSilva, for their help with magnetic measurements and interpreting magnetic data; Christopher Kareis, for many discussions on procedure and methodology; Endrit Shurda, for help with infrared spectroscopy and interpretation; Josh Sussman for assistance with EDS; all members of Dr. Miller's research group, for their friendship and support.

Thanks go to Dr. Ashutosh Tiwari and Dr. Michael Scarpulla, for being on my committee, and for their confidence in me; the Materials Characterization Lab, for allowing me to use the scanning electron microscope; Nathan Gray and Jason Stoker, for their friendship and support; the Department of Energy for funding.

Thanks go to my wife, Kristyn, and my son, Bryce, for putting up with me while in graduate school, and for always being there with support and understanding when things were hard; to all of my family, for their continued support and for instilling in me a wonder for the world and a need to continue discovering for all of my life.

CHAPTER 1

INTRODUCTION

Magnets are an integral part of modern technology. Advances in research on magnets and magnetic phenomena drive progress in many technological fields, including popular consumer-geared products like sound systems and computer data storage. As the range of products demanding high magnetic performance increases, especially in new and unexpected environments, there is a need to find novel magnetic materials that can fill new criteria and excel under diverse conditions. These materials must have comparable or superior magnetic properties to traditional magnets and should be as easy or easier (including cost and energy considerations) to manufacture. The following literature review outlines the origins and principles of magnetism relevant to this thesis, as well as specific materials and issues leading up to the development and realization of this project.

Literature Review

Magnetism

The phenomenon of magnetism was first observed several millennia ago.[1] Only relatively recently, however, has a fundamental understanding of magnetism and its behaviors been established due to quantum mechanics. In-depth quantum theories and

mathematical models are beyond the scope of this paper,[2] but an introduction to a few basic concepts in magnetism applicable to this project are included.

The essential component to magnetism lies in the spin associated with an unpaired electron.[3] Atoms (and molecules) have energy states, called orbitals, which are occupied by electrons. Every electron has a specific set of four quantum numbers that is unique from all other electrons in an atom. One of those numbers is the spin quantum number with possible values of either +1/2 (spin up) or -1/2 (spin down). For this reason, each orbital can only accommodate two electrons, one spin up and one spin down. Electrons fill orbitals from low energy to high energy and will generally fill each with two electrons. The spins of these two electrons oppose each other with regard to how they interact with an external magnetic field, and materials with only paired electrons are termed diamagnetic, meaning they will weakly repel a magnetic field. When there are unpaired electrons, they interact with and are weakly attracted to an applied magnetic field. Materials with unpaired electrons are termed paramagnetic.

How these unpaired electrons interact with each other depends on the material. The first question is whether or not the material will order magnetically, and if it does, does it exhibit ferromagnetic or antiferromagnetic coupling. Ordering occurs when spins within the material overcome their random alignment and strongly couple with each other.[3] If the coupling becomes great enough, the sites will more or less all align in the same direction in a magnetic field, and when this happens, the material is “ordered” magnetically.

For materials that do order, there is a temperature called the critical temperature, T_c, which is the temperature at which the electron spins will align themselves (parallel or antiparallel) into an ordered system. If a material does order, there are three main types of magnetic ordering it can display, as shown in Figure 1.1. The first is ferromagnetism, where all spin sites align themselves parallel to each other and point in the same direction.

The second is antiferromagnetism, where spin sites align themselves antiparallel to each other, meaning they point in opposite directions.[6] The difference between the two is that in the ground state, at zero kelvin and in zero applied field, an antiferromagnet would show no magnetism because the oppositely aligned magnetic moments would exactly cancel each other, whereas the ferromagnet would show a strong magnetic field due to the alignment of the spin sites. Above T_c, however, even antiferromagnets display a magnetic response due to thermal energy and other factors.[6]

The third type of magnetic ordering is called ferrimagnetism. This occurs when spin sites align themselves antiparallel as in antiferromagnets, but the magnitude on one type of spin site is not equivalent to the other, as shown in Figure 1.1. In this case, there is a larger magnetic moment in one direction than the other, giving it a net magnetic moment. How a magnetic material orders is important, but equally important is, once magnetized, how it behaves in an applied magnetic field. Included in this aspect of magnetic behavior are hysteresis and coercive field, the two most important concepts of magnetism to this project.

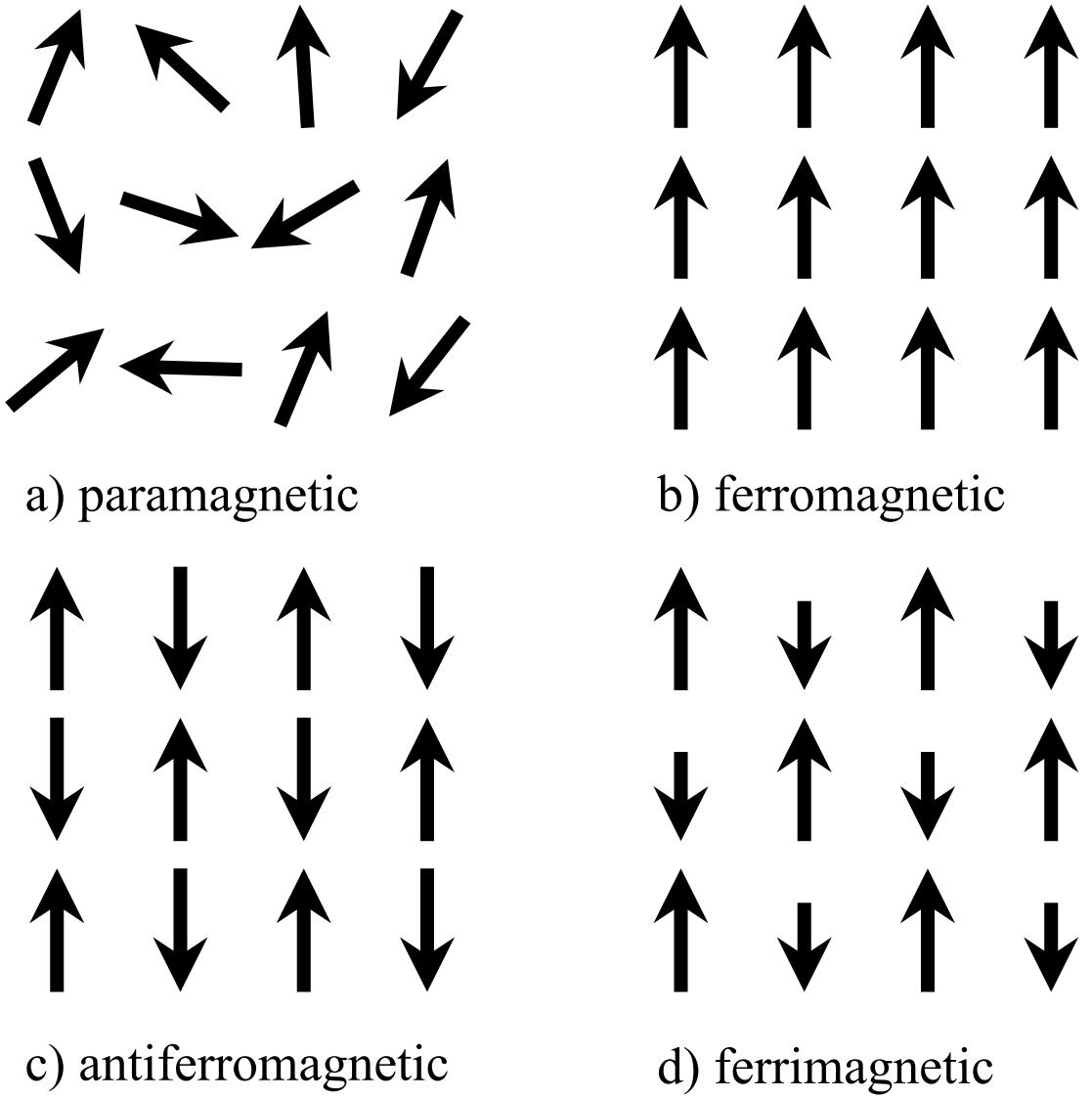

Figure 1.1: Illustration of different types of magnetic behavior. a) Paramagnetic behavior where the material has unpaired electrons but no ordered alignment. b) Ferromagnetic ordering where all spin sites align in the same direction and parallel to each other. c) Antiferromagnetic ordering where the spin sites align antiparallel to each other and have equal magnitude. d) Ferrimagnetic ordering, where spin sites align antiparallel and have unequal magnitude.

Hysteresis and Coercive Field

The coercive field of a magnetic material is the measure of how resistant it is to a reverse magnetic field that would demagnitize the sample.[3] An easy way to visualize the coercive field is to look at a typical hysteresis loop, shown in Figure 1.2. To create the hysteresis loop, a sample starts at the origin with no intrinsic magnetization and zero applied magnetic field. A magnetic field, H, is then incrementally applied and the sample begins to interact with the field, its electron spins aligning with the applied magnetic field to magnetize the sample. Ideally, at some point, the sample will reach a saturation point, M_s, at which there is no more potential for the material to increase in magnetization with an increased applied field. The applied field is then incrementally reduced back to zero, and a negative field of equal magnitude to the positive field is applied. It is then reversed and taken to the maximum positive applied field again to complete the loop. If the sample displays hysteretic behavior (meaning that it does not return to the origin), there are two points of interest.

The first is the remnant magnetization, M_r, or how magnetized the sample is when the applied field returns to zero. Another point is the coercive field, H_{cr}, measured in Oersted (Oe). Essentially, when the sample is saturated, it would require a reverse magnetic field of magnitude equal to the coercive field to return the sample to zero magnetization. Materials with a high coercive field (>100 Oe) are termed "hard" magnets and are used in applications demanding a more permanent magnetization, such as in the hard drive of a computer. Alternatively, materials with a low coercive field (<10 Oe), or "soft" magnets, are used in applications where sensitivity to small magnetic

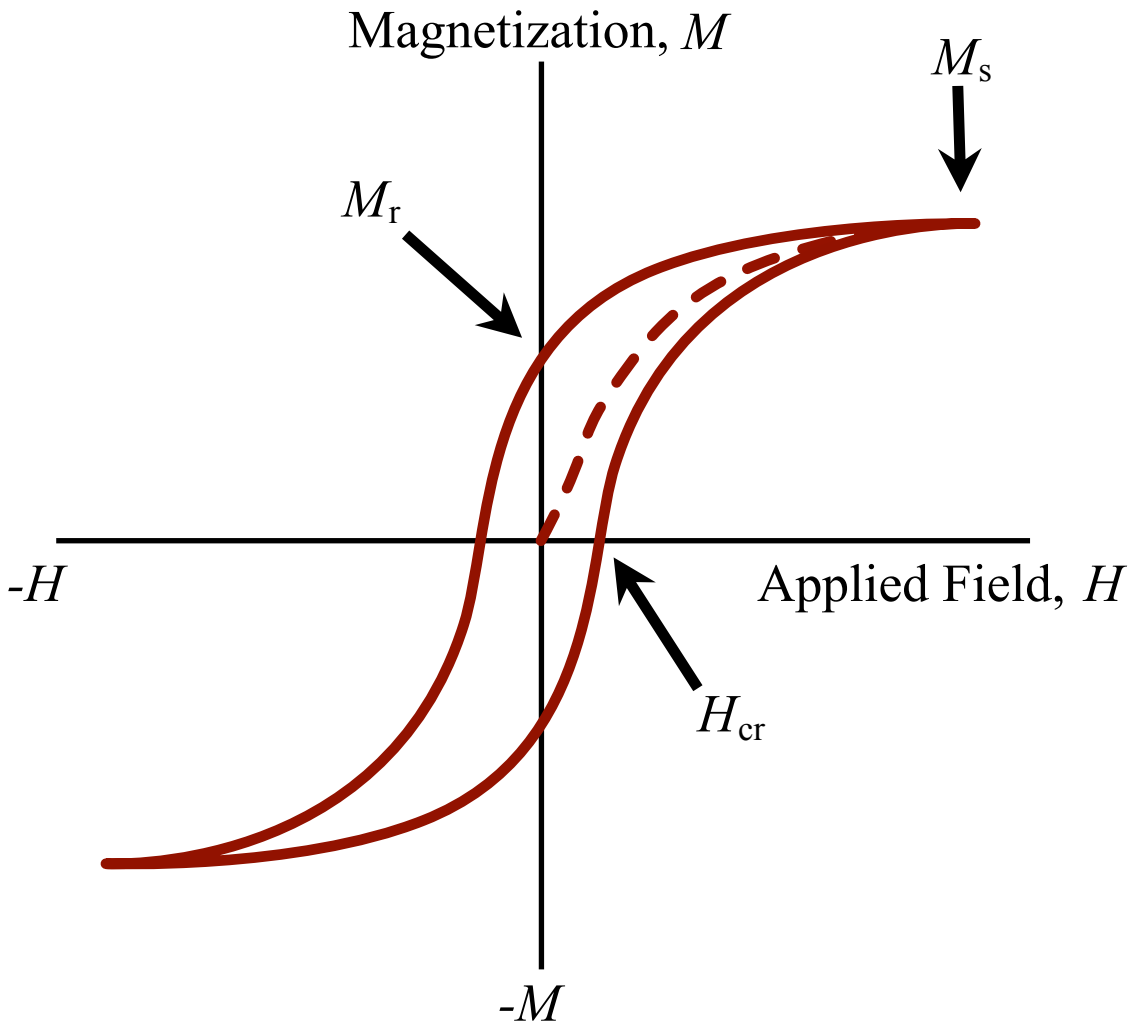

Figure 1.2: A typical magnetic hysteresis loop. The virgin curve rises from the origin to the saturation magnetization, M_s, but when the applied field is incrementally taken back to zero the magnetization does not return to zero, but a remnant magnetization, M_r remains. The applied magnetic field in the opposite direction required to return the material's magnetization to zero is called the coercive field, H_{cr}.

changes is important, such as in voltage transformers for AC current, where a higher coercive field leads to greater energy loss each time the current is reversed. The material components of a magnet have a big effect on the coercive field, and that is an important consideration in finding new magnetic materials.

Molecule-Based Magnets

Traditional magnets are made of metals or ceramics. These materials can have high critical temperatures making them good room-temperature magnets, but they also require high-temperature processes to make, which are simple but high in energy cost and often high in material cost as well. It was advantageous to identify new magnetic materials that could be processed at low temperatures and still exhibit similar properties to traditional magnetic materials. Furthermore, any new class of materials discovered with certain properties – magnetic, electrical, etc. – opens the door for new and improved applications. For these and other reasons, research in new magnetic materials was started, especially in the realm of organic-based magnets.

The idea that there could be organic-based magnetic materials stemmed from the discovery of metal-like electrical conductivity in some organic materials.[4] One material in particular provided a breakthrough: $[Fe^{III}Cp^*_2][TCNQ]$ where TCNQ = 7,7,8,8-tetracyano-*p*-quinodimethane and Cp* = pentamethylcyclopentadiene (Figures 1.3a and 1.3b, respectively). This material exhibited two magnetically ordered phases, one being antiferromagnetic in the ground state and ferromagnetic in an applied field, and the other ferromagnetic in the ground state. Each ion has one unpaired electron. In an attempt to

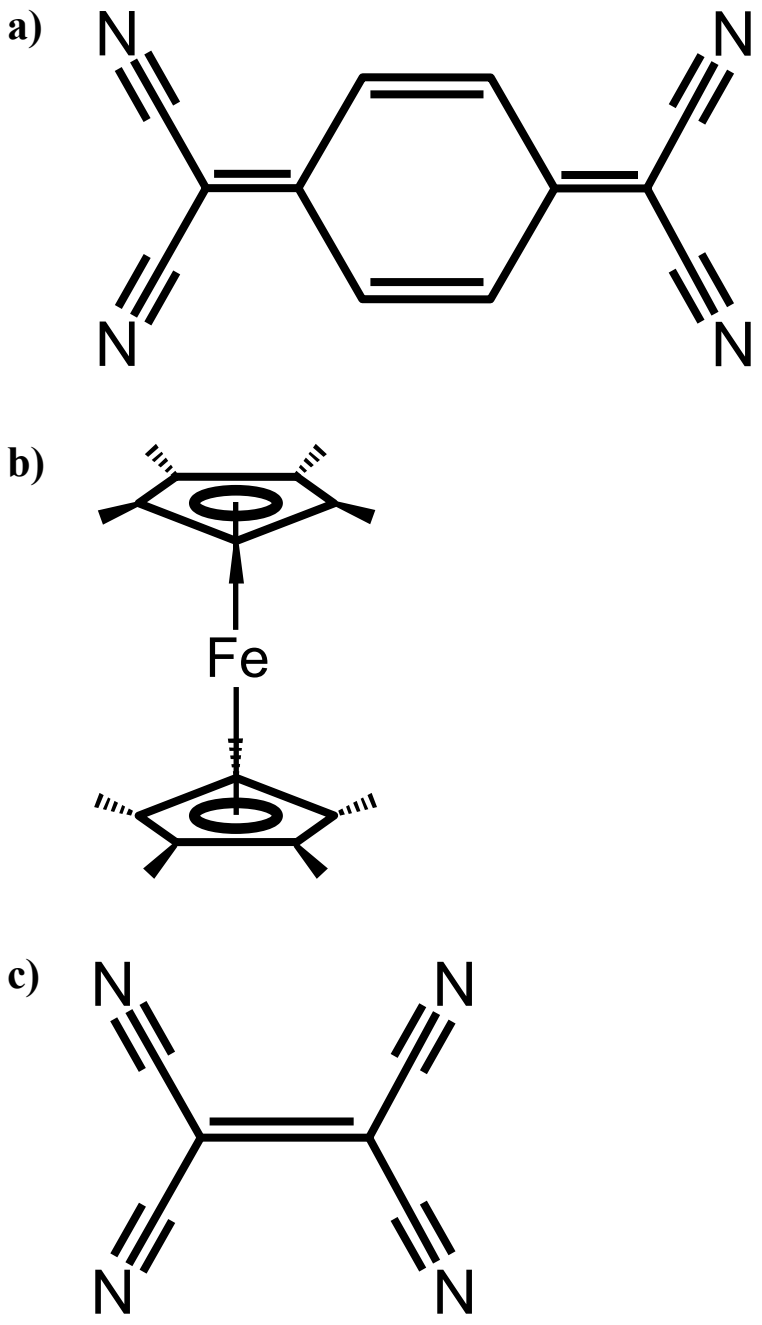

Figure 1.3: Structures of a) 7,7,8,8-tetracyano-*p*-quinodimethane (TCNQ), b) decamethylferrocene ($FeCp^*_2$), and c) tetracyanoethylene (TCNE).

stabilize the ferromagnetic state, a molecule similar to, but smaller than, TCNQ was used in its place. Tetracyanoethylene (TCNE), shown in Figure 1.3c, was identified, resulting in $[Fe^{III}Cp^*_2][TCNE]$, which showed the desired results, having a ferromagnetic ground state.[5] The only limitation to this new material was its extremely low value of T_c at 4.8 K. These organic-based magnets were novel and it was surprising that they exhibited magnetic behavior, but to become a viable substitute to traditional magnets in technological applications, the critical temperature needed to be higher than room temperature (~300 K).

$V[TCNE]_2$

Different metal atoms were substituted in the structure above which led to the discovery of $[Mn^{III}Cp^*_2]^+[TCNE]^{\bullet-}$ with a T_c of nearly 9 K, at the time a very high T_c for a molecule-based magnet.[6] Knowing that $V^0(C_6H_6)_2$ has a similar electronic structure to $Mn^{III}Cp^*$, Miller and coworkers reacted it with TCNE to hopefully attain a similar or slightly higher T_c.[7] To their surprise, they not only created a molecule-based magnet, but one that was magnetic at room temperature.

$V[TCNE]_2$ measured a T_c above 350 K, making it a magnet at room temperature.[8] The coercive field was measured as 0.2 ± 0.1 Oe at 300 K to 7.8 ± 0.1 Oe at 2 K.[9] These values place $V[TCNE]_2$ as a soft magnet, limiting its potential applications. Further adding to this compound's limitations were two facts: (1) it is pyrophoric, meaning it will combust (or at the very least, decompose) if exposed to oxygen and (2) as prepared from

dichloromethane (CH_2Cl_2) the material thermally decomposed around 350 K, making a determination of the true T_c difficult and any application above 350 K unattainable.[9]

In response to the thermal degradation of the material, different solvents were considered in place of CH_2Cl_2. It was found that some solvents adversely affected the T_c, lowering it below room temperature.[10] Others were shown to thermally stabilize the material while not affecting T_c. However, this did not eliminate the pyrophoric property of the material.

A chemical vapor deposition (CVD) technique was developed to produce a thin film of the material.[11] The ability to make $V[TCNE]_2$ directly from precursors in the vapor phase eliminated the necessity for a solvent altogether and a purer material resulted with no effects from solvent inclusion in the structure. The film was also found to be relatively more air stable than the bulk powder samples. To further protect the film from the deleterious effects of air, a transparent, Parylene polymer coating was devised for the film that would be relatively impermeable to air but would not affect the magnetic properties.[12] Neither of the above methods (solvent enhancement or thin-film deposition) solved the issue of $V[TCNE]_2$ being a soft magnet, however.

$V_xCo_{1-x}[TCNE]_2$

As a solution to the limitation of having a small coercive field, Miller et al. proposed the substitution of some of the vanadium in $V[TCNE]_2$ with cobalt, making a substitutional alloy $V_xCo_{1-x}[TCNE]_2$.[13] Cobalt(II) ions are known to contribute a large magnetocrystalline anisotropy, which is a key cause of coercive field, when substituted in

small amounts for other metallic ions, as in manganese ferrite ($MnFe_2O_4$).[3] When cobalt was substituted in small amounts for manganese in this compound in concentrations as little as $Mn_{0.9}Co_{0.1}Fe_2O_4$, the anisotropy constant was changed by an order of magnitude. This provided adequate justification for the hope that cobalt in $V[TCNE]_2$ would increase the coercive field. What was found when substituting cobalt in $V[TCNE]_2$ is shown in Figure 1.4.[13] All measurements were taken at 5 K. First, in the upper left-hand corner is a hysteresis loop for a physical mixture of $V[TCNE]_2$ and $Co[TCNE]_2$. As seen, the coercive field of this mixture is the same, or close to that of pure $V[TCNE]_2$, indicating that any effects seen by the addition of cobalt in a substitutional alloy are real and not just those of a physical mixture. The main body of the plot shows several hysteresis loops measured for $V_xCo_{1-x}[TCNE]_2$ at various compositions of x. Though the graph is cluttered, it is clearly evident that where any cobalt is present in the compound, the coercive field far exceeds that of pure $V[TCNE]_2$ or the physical mixture of both. Further, in the lower right-hand corner of the plot is an inset showing the coercive field with respect to vanadium concentration, x. The points at $x = 1.0$ and $x = 0.0$ were manually added as a guide for establishing a trend. The effect of cobalt addition on coercive field reaches a maximum where $x = 0.3$, with a coercive field of approximately 280 Oe.

$Co[TCNE]_2$

Little had been done as far as $Co[TCNE]_2$ is concerned because it was found to be paramagnetic with no magnetic ordering.[13] One report indicates that a $Co[TCNE]_2$ thin-

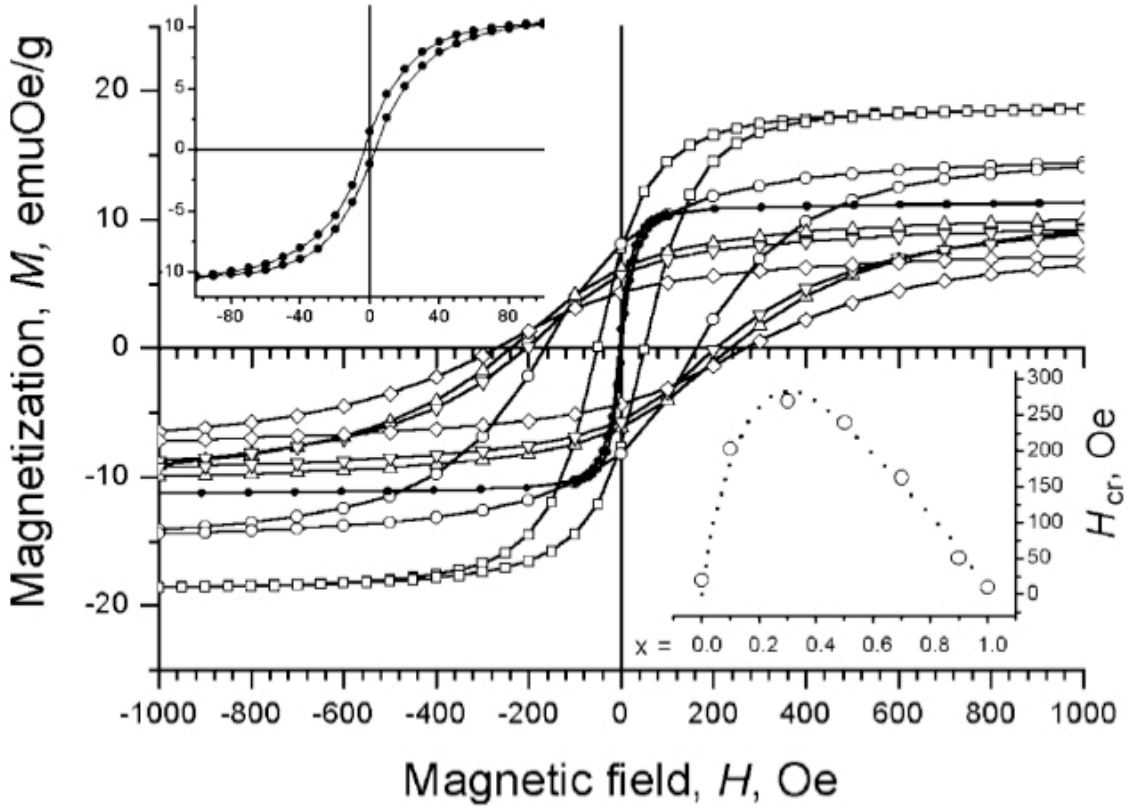

Figure 1.4: Hysteresis loops at 5 K for the $V_xCo_{1-x}[TCNE]_2 \cdot zCH_2Cl_2$ ($0.1 \leq x \leq 0.9$) solid solutions (x = 0.9, □ ; x = 0.7, ○ ; x = 0.5, △ ; x = 0.3, ▽ ; x = 0.1, ◇), and physical mixture consisting of $V[TCNE]_2 \cdot zCH_2Cl_2$ and of $Co[TCNE]_2 \cdot zCH_2Cl_2$ in 1:1 ratio (●). The top left inset shows the physical mixture data in a smaller scale, and the bottom right inset shows the coercive field, H_{cr}, dependence upon x (line is a guide for the eye).[13]

film had been made but no details on the conditions of the experiment were given and no attempt to explain the data was made.[14]

Infrared Spectroscopy

TCNE. Much has been done to identify the infrared (IR) characteristics of TCNE, as the cyanide (C≡N) stretch in TCNE (Figure 1.3c) is IR visible and highly sensitive to structural properties and formal charge.[15] The typical absorptions in the IR of many different structural and ionic forms of TCNE are shown in Figure 1.5. If one knows the structure and charge of a specific TCNE-containing compound, one should be able to predict where the peaks will fall in the IR spectrum, and vice-versa. Realistically, much ambiguity arises due to the fact that the peak intensities and the decision to report shoulders as well as peaks were matters of preference for the several researchers whose data are represented in this map.[15] Furthermore, if more than one conformation of TCNE is present in the compound, peaks may overlap or obscure one another, creating more difficulty in narrowing down specific phases present in the material. However, one major trend is evident from these data: the average absorption in the cyanide region will fall into a certain zone, depending on the charge, z, on the $[TCNE]^z$ molecule. If the TCNE is neutral (z = 0), the average absorption will occur above 2210 cm^{-1}; for z = 1-, between 2210 and 2150 cm^{-1}; and for z = 2-, below 2150 cm^{-1}.[15] Thus, at the least, the charge on the TCNE can be determined and can show that TCNE has reacted and been reduced.

$V_xCo_{1-x}[TCNE]_2$. Infrared spectroscopy is an important way of characterizing the mixed films of varying composition. As this region is highly sensitive to structure and

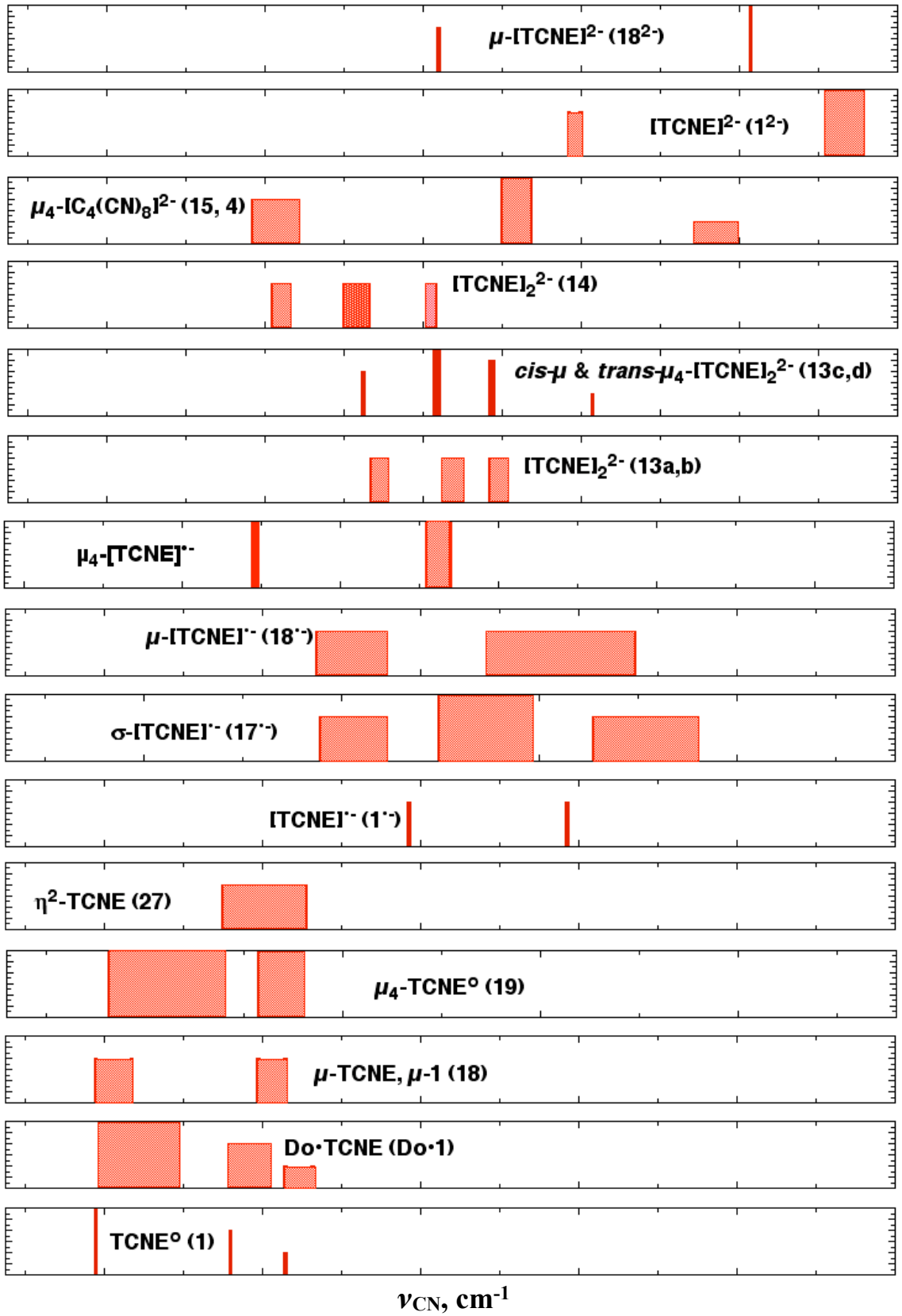

Figure 1.5: ν_{CN} absorption ranges for structurally characterized forms of TCNE.[15]

composition (see above), the differences in vanadium and cobalt concentrations should reveal subtle differences in the IR. Figure 1.6 shows the composition range from $x = 0.0$ to $x = 1.0$ and their accompanying IR spectra.[13] Note that the x-axis increases in wavenumber left-to-right, which is opposite the traditional notation. The most readily noticeable feature of this plot is the shift in energy of the most intense peak, from 2152 cm^{-1} in pure $V[TCNE]_2$ to 2171 cm^{-1} in pure $Co[TCNE]_2$. Other transitions, while present, are less prevalent and more ambiguous to define.

Project Motivation and Goals

The motivation and goals for this project were two-fold. First, $Co[TCNE]_2$ had not been fully explored as a thin-film material. Thus, the development and identification of a reproducible CVD route was sought. Obtaining the IR and magnetic data for these thin-films was necessary to compare with available bulk material data as well as establish a base line for future exploration into this material, as current research shows that there may be magnetically ordered phases or solvent complexes of this material.[16]

The second, and by far the larger priority of the project, was the deposition and characterization of films with varied composition of vanadium and cobalt in the form $V_xCo_{1-x}[TCNE]_2$. In powder samples, the addition of cobalt has been shown to increase the material's coercive field, and the coercive field appears to be tunable based on the amount of cobalt in the substitutional alloy. Successful deposition of $V_xCo_{1-x}[TCNE]_2$ as a thin-film would allow the enhanced magnetic properties to be available in a form of the material that could also be protected from oxygen via a polymeric coating.

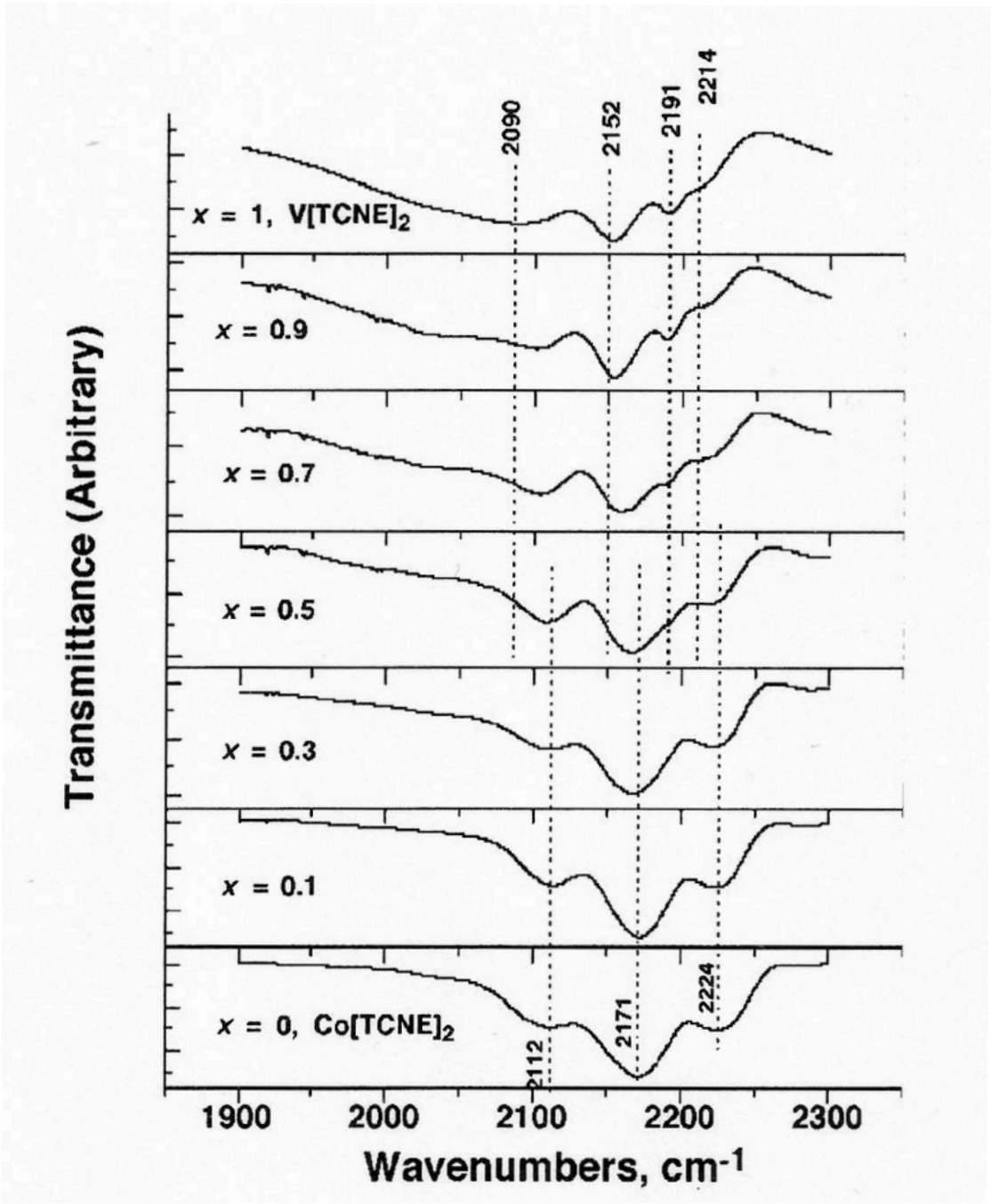

Figure 1.6: ν_{CN} IR spectra of $V_xCo_{1-x}[TCNE]_2 \cdot zCH_2Cl_2$ ($0 \leq x \leq 1$).[13]

CHAPTER 2

SINGLE-METAL TCNE FILMS

The procedure for synthesizing $V[TCNE]_2$ thin-films is known.[17] Not all conditions and details are reported in the literature, however, but are recorded in laboratory notebooks. Supplementary information was received by contacting the individuals who conducted research on this material. That procedure and the accompanying apparatus design were adapted to successfully implement deposition of $Co[TCNE]_2$, and the resultant films have been characterized by infrared spectroscopy as well as on the magnetometer.

$Co[TCNE]_2$

Experimental

Starting materials. Crude tetracyanoethylene (TCNE) and cobalt carbonyl ($Co_2(CO)_8$) were obtained commercially and required purification by sublimation before use. The TCNE was sublimed under static vacuum in a water-cooled sublimator at 60 °C. Sublimation of ~15 g of TCNE took approximately three days to go to completion. Sublimation removes water and any other contaminants from the TCNE, resulting in clear crystals (any yellow tint would indicate the continued presence of water and would

require a second sublimation) which are then stored in an inert atmosphere to protect them from future water contamination. The $Co_2(CO)_8$ was sublimed in an ice-cooled sublimator under static vacuum at room temperature for approximately seven hours. Care was taken to make sure the $Co_2(CO)_8$ was not ever exposed to air by sealing the sublimator under vacuum inside a nitrogen-filled glove box before sublimation. Furthermore, the seal was not broken until the $Co_2(CO)_8$ was collected in the glove box. The $Co_2(CO)_8$ crystals were bright orange, and were stored in a freezer at -20 °C to prevent them from thermal degradation. The materials were then ready for use in deposition.

Chemical vapor deposition apparatus. Due to the novelty and small scale of this project, a unique apparatus was designed and implemented for chemical vapor deposition (CVD). The glassware was tested rigorously both outside and inside the glove box in which all depositions would occur to confirm that appropriate vacuum levels, flow rates, and temperatures were attainable. The final apparatus for depositing single-metal TCNE films is shown in Figure 2.1.

The glass CVD tube was approximately 20 in long and had a diameter of 1.3 in. The inside tubes had a diameter of 1 cm and met in the middle with a 0.5 in gap between them. A resistive heater (Watlow Thinband C/NSTB1G3J1-A12) wrapped around the outer chamber over the TCNE boat, and a thermocouple (OMEGA Chromel Alumel Type K) attached to the outside of the glass near this heater monitored and controlled its temperature via a temperature controller (Red Lion Model T-16 Temperature/Process Controller). The T-shaped glass holder for the $Co_2(CO)_8$ was submerged in a silicon oil

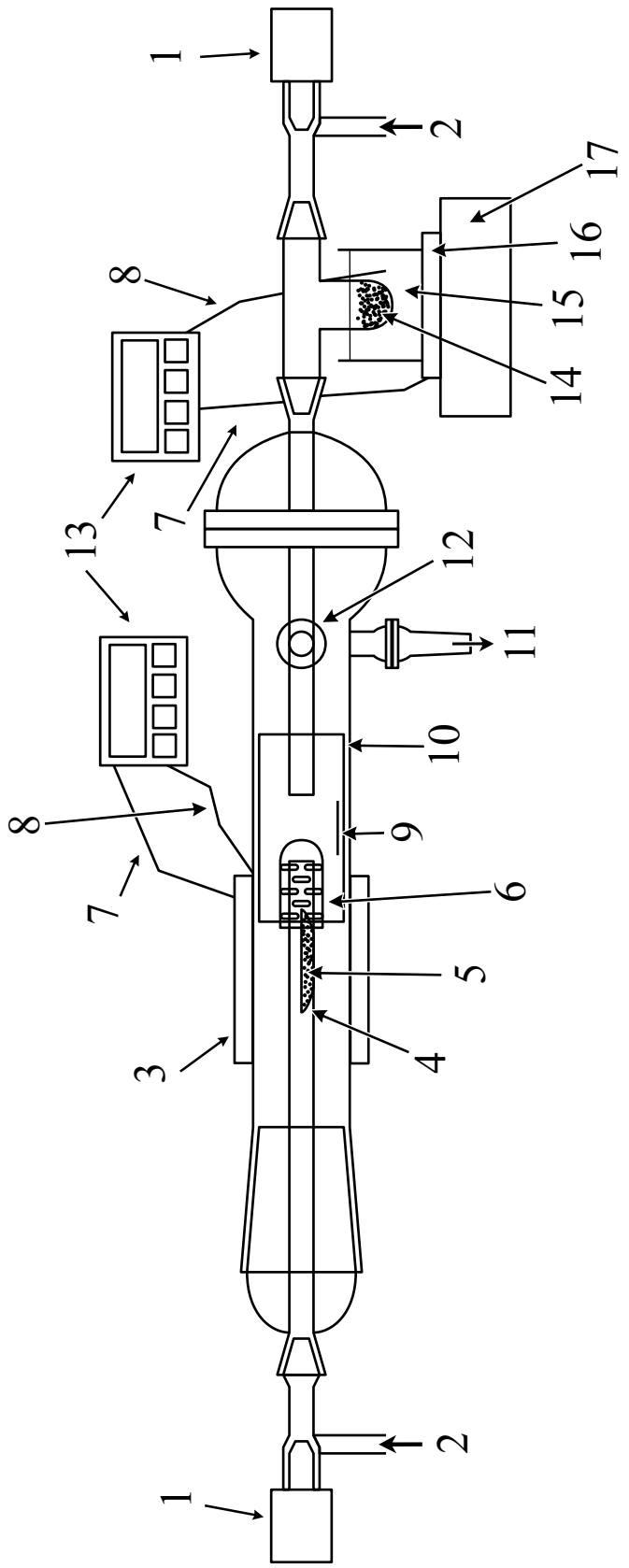

1) Flow Valves
2) N_2 In
3) Resistive Heater
4) TCNE Boat
5) TCNE
6) Flow Cap
7) Control Wires
8) Thermocouples
9) Substrate
10) Substrate Holder
11) Vacuum Out
12) To Vacuum Gauge
13) Temperature Controllers
14) $Co_2(CO)_8$
15) Silicon Oil Bath
16) Peltier Cooling Unit
17) Heat Sink and Fan

Figure 2.1: The chemical vapor deposition apparatus for single-metal thin-films.

bath mounted on a Peltier cooling unit, which uses the thermoelectric effect to achieve adequately low temperatures.[18,19] Another thermocouple rested in the silicon oil to monitor and control that temperature as well. Substrates for film deposition were mounted in a square glass tube and centered in the deposition chamber for maximum exposure to the deposited film. A hose was connected to an Edwards E2M5 two-stage vacuum pump outside the glove box which pulled nitrogen from the box through the deposition chamber and out the vacuum line. This created both the necessary nitrogen flow to carry the vapors to the center of the chamber as well as a sufficient vacuum level inside the chamber with a minimum value of 10 torr. With this equipment set up and ready inside the glove box, the system was ready for film deposition.

Chemical vapor deposition. TCNE was placed in a small glass boat on the left side of the chamber, and $Co_2(CO)_8$ in a T-shaped glass boat on the right, as shown in Figure 2.1. The TCNE was heated to 45-55 °C (depending on the run), ensuring sublimation inside the chamber, and the $Co_2(CO)_8$ cooled to 10 °C to maintain an acceptable rate of sublimation. Nitrogen flow (measured in standard cubic centimeters per minute, SCCM) carried the sublimed TCNE at 120-150 SCCM and the $Co_2(CO)_8$ at 100 SCCM to the center of the tube where they reacted and deposited on the substrates. At first, microscope slide glass (VWR) was cut into squares roughly 1/8” to a side and mounted with grease in the square tube substrate holder. Attempts to characterize these films magnetically failed and led to the conclusion that the glass was too thick and there was not enough film on them to register a magnetic signal. To correct this issue, microscope cover slides (VWR micro cover glass) were used in the place of the slides

themselves. The cover slides (~3/4" to a side) were placed in the substrate holder whole, and were large enough to not need grease to hold them in place. Potassium bromide (KBr) plates were used as substrates for infrared spectroscopy characterization in all films.

The vapor phase reaction of TCNE and $Co_2(CO)_8$ should follow the formula:

$$4TCNE\ (v) + Co_2(CO)_8\ (v) \rightarrow 2Co[TCNE]_2\ (s) + 8CO(g) \qquad (2.1)$$

A stoichiometric amount of these starting materials was measured out for the first few films, but the precursors did not sublime at proportional rates to accommodate the stoichiometry, so when one component was exhausted, the other would still sublime and could possibly deposit on top of the film as a contaminant. It was determined that the best method was to interrupt the deposition before either material was exhausted to maintain the stoichiometry of the film. Thus, there was no need to accurately measure the starting materials beforehand. Instead, between 50 to 75 mg of $Co_2(CO)_8$ and around 100 mg of TCNE were used in the CVD apparatus, which would deposit between 1 and 2 mg of film on the 3/4" glass slide over about four hours of deposition.

The deposition parameters of eight $Co[TCNE]_2$ films are listed in Table 2.1. Films **1a-f** were deposited on the thicker microscope slide glass, whereas films **1g-j** were deposited on cover slide glass in order to provide less noise in magnetic characterization.

Characterization. Infrared spectroscopy data were collected on a Bruker Tensor 37 Infrared Spectrometer, with scans from 400 to 4000 cm^{-1} ($\pm 1\ cm^{-1}$). KBr was used as

Table 2.1
Deposition parameters for $Co[TCNE]_2$ films.

Film	Notebook Number	Temperature of TCNE* (ºC)	Temperature of $Co_2(CO)_8$* (ºC)	Flow Rate over TCNE‡ (SCCM)	Flow Rate over $Co_2(Co)_8$‡ (SCCM)
1a	PKE01-095	55	10	150	100
1b	PKE01-097	55	10	150	100
1c	PKE01-099	50	10	120	100
1d	PKE01-149a	55	10	150	100
1e	PKE01-149b	55	10	150	100
1f	PKE01-109	50	10	120	100
1g	PKE01-111	50	12	120	100
1h	PKE01-113	50	10	120	100
1i	PKE01-127	45	10	120	100
1j	PKE01-139	45	10	120	100

* ±3 ºC
‡ ±5 SCCM

the substrate for all IR measurements. Each film was measured after deposition was complete. To measure the effect of time and air exposure on the film, one sample (film **1b**) was measured multiple times up to a week after deposition, and then exposed to air and measured several more times.

Magnetic data were collected on a Quantum Design MPMS 5T SQUID magnetometer. The films deposited on glass, both microscope slides and cover slides, were used in the magnetic measurements. The film-covered glass slides were packed into gelatin capsules (glass wool was used with the original microscope slides to prevent them from moving) during measurements. Measurement of the magnetic susceptibility with respect to temperature of the films was taken from 5-300 K. Also measured on the magnetometer for some films was the magnetization versus the applied field, and for only samples **1i** and **1j**, magnetic hysteresis.

Results and Discussion

Film deposition. Each deposition situation outlined in Table 2.1 successfully deposited a film. Neither the run time for the depositions nor the amount of starting material had any significant effect on the resulting amount of film. As discussed, film deposition was interrupted before either starting material was exhausted in all films except for the first two in order to prevent potential contamination by unreacted material. For films **1a** through **1e**, with the exception of **1c**, the temperature and flow rate on the TCNE side were set to 55 ºC and 150 SCCM, respectively. In these films, the TCNE sublimed quickly and moved too fast through the deposition zone. This resulted in some

deposited film, but incurred a large loss of TCNE, either through the vacuum pump or deposited along the walls of the deposition tube. For films **1c** and **1f-h**, the flow rate over TCNE was decreased to 120 SCCM and the temperature of the TCNE was decreased to 50 ºC. This increased the yield of actual film, and decreased the waste of TCNE, but still exhibited some waste in the form of excess TCNE. The final two $Co[TCNE]_2$ films, **1i** and **1j**, were further cooled to 45 ºC on the TCNE, which effectively eliminated observable waste while maintaining good yield on the films.

Infrared spectroscopy. The samples deposited on KBr plates were used in infrared spectroscopy (IR). The IR spectra for all cobalt films except for film **1d**, **1e** (for which data is not shown), and **1j** (for which no KBr pellet was prepared) are shown in Figure 2.2. All of the films exhibited similar spectra, with only slight variations in relative intensities of peaks and shoulders. The key region in the IR for chemistry involving TCNE is the C≡N region as discussed previously, which exhibits characteristic absorptions based on the different ionic character of TCNE and how it is coordinated to other atoms.[15] All of these absorptions occur in the 2000-2300 cm^{-1} range and shifts in these peaks indicate changes in composition and structure.

The IR spectrum of bulk $Co[TCNE]_2$ is shown in Figure 1.6. This IR shows absorption peaks at 2224 and 2171 cm^{-1}, as well as a shoulder at 2112 cm^{-1}. The spectra of the cobalt films in Figure 2.2 show sharp absorption peaks at 2225 and 2172 cm^{-1}, with a shoulder at about 2110 cm^{-1}. Thus, the data from these thin-films match data from the bulk samples that have been reported.

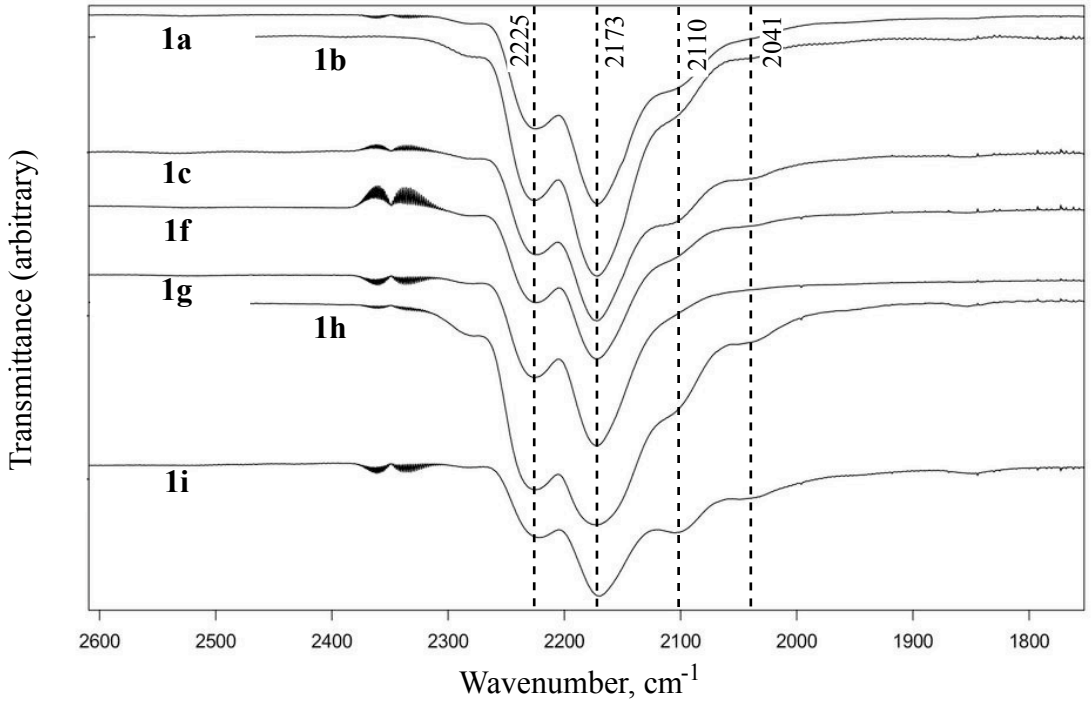

Figure 2.2: Infrared spectra of $Co[TCNE]_2$ thin-films. Dotted lines are guides for the eye.

A study was also done on how the film held up after time and when exposed to air. An IR spectrum was taken of film **1b** incrementally for nine days after deposition, and then for two days after exposure to air. The key region with the effects of time and air on the film are displayed in Figure 2.3. After nine days, the spectra show no noticeable differences. After just two hours in air, however, the shoulder located at about 2110 cm^{-1} began to disappear. Furthermore, the two major peaks shifted slightly as can be seen in Figure 2.3. The absorptions shifted from 2225 and 2172 cm^{-1} to 2222 and 2177 cm^{-1}, respectively. Although not a very large shift in values, this shift, along with the disappearance of the shoulder, indicates the beginning of a change in the film due to decomposition, or perhaps a slight shift in the structure of the film.

$Co[C_4(CN)_8]$. $Co[TCNE]_2$ from solution is reported as paramagnetic with no magnetic ordering, but with cobalt's ability to increase coercive field in a material and a similarly composed $V[TCNE]_2$ material exhibiting room temperature magnetism, it stood to reason to investigate further into why this material showed only paramagnetic behavior.

Recent research has shown that several different routes can be employed to synthesize what should result in bulk $Co[TCNE]_2$ from solution.[16] The first is the reaction of $Co_2(CO)_8$ in a dichloromethane (CH_2Cl_2) solution with TCNE, the most analogous route to the vapor phase CVD reaction of the same components. The second is the reaction of cobalt thiocyanate [$Co(NCS)_2$] and tetrabutylammonium tetracyanoetylene (NBu_4TCNE), also in acetone ($OCMe_2$). The third is the reaction of

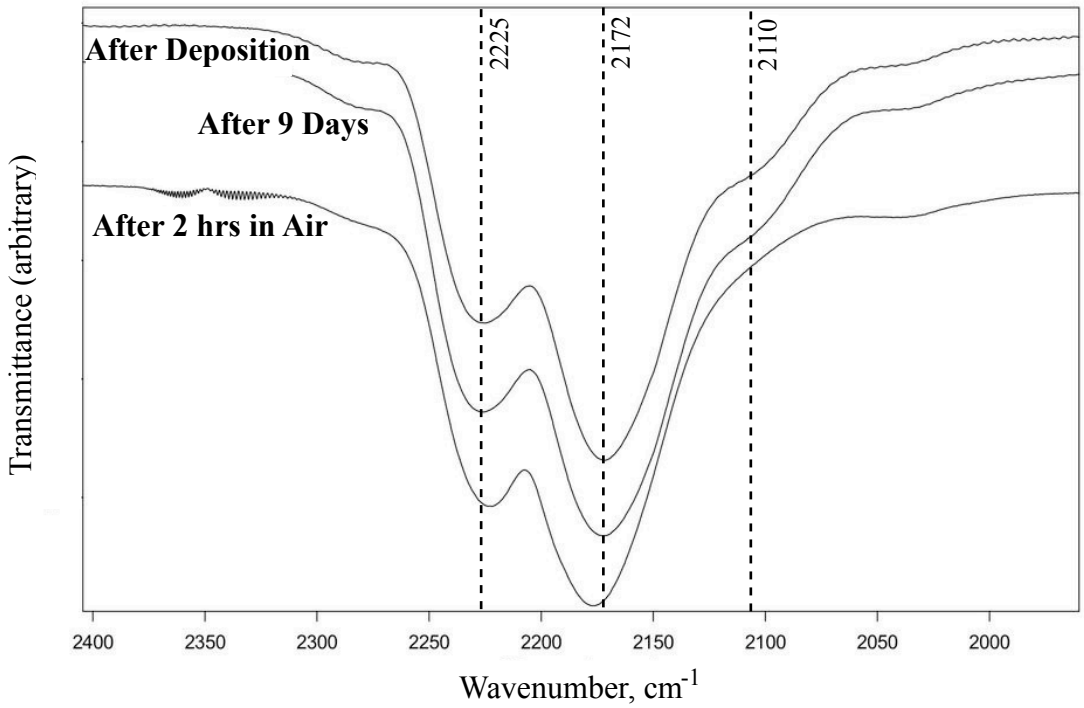

Figure 2.3: Infrared spectra of film **1b** exhibiting changes to IR after exposure to air. Dotted lines are guides for the eye.

bis(acetonitrile)diiodocobalt(II) ($CoI_2(NCMe)_2$) and TCNE in acetonitrile (MeCN). The fourth is the same as the second, but in CH_2Cl_2 instead of acetone.

The carbonyl route yielded a black, amorphous powder that could not be structurally characterized. The second route yielded crystals characterized as $Co[C_4(CN)_8](OCMe_2)_2$. $[C_4(CN)_8]^{2-}$ is a dimer that forms from TCNE, pictured in Figure 2.4. Upon annealing the acetone was removed, resulting in $Co[C_4(CN)_8]$. The third route yielded $Co[TCNE][C_4(CN)_8]_{1/2}$, the only one to have TCNE still in the structure. The fourth yielded $Co[C_4(CN)_8](NCMe)_2$, a solvated compound with only the dimer present again. It is unresolved whether or not the latter two compounds exhibit more than simply paramagnetic behavior, but their magnetic behavior is different than that of the first route and the thin-films.

The IR spectra of the products of these four reactions are compared with film **1i** in Figure 2.5. The IR spectra indicate that the cobalt carbonyl synthetic method is identical to the thin-films. These two products, though amorphous, are very similar in IR to the $Co[C_4(CN)_8](OCMe_2)_2$ from solution, as well as this compound when desolvated. The latter two products are quite different in the IR from the first three. These IR data indicate that the films may not contain TCNE radical anions but the TCNE dimer, $C_4(CN)_8$, instead. This consideration will be important when interpreting the magnetic data of these $Co[TCNE]_2$ thin-films and in comparing them with $V[TCNE]_2$ films.

However strong the evidence for these films being $Co[C_4(CN)_8]$, the cobalt-containing films will still be referred to as $Co[TCNE]_2$ throughout the remainder of this report to maintain consistency.

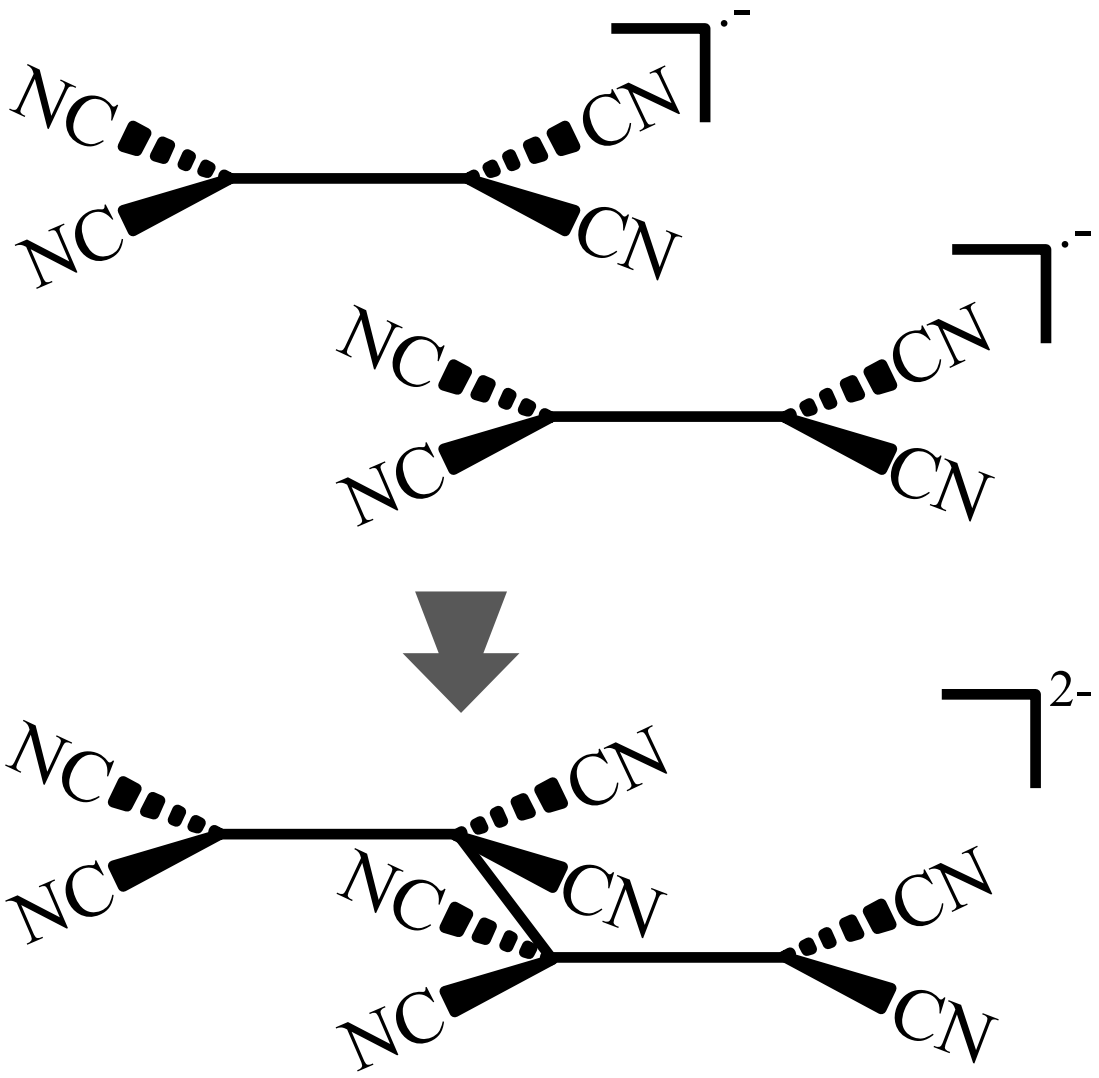

Figure 2.4: Illustration of the formation of the TCNE dimer, $C_4(CN)_8$, where two TCNE radical anions combine to form a stable dimer with no unpaired electrons.

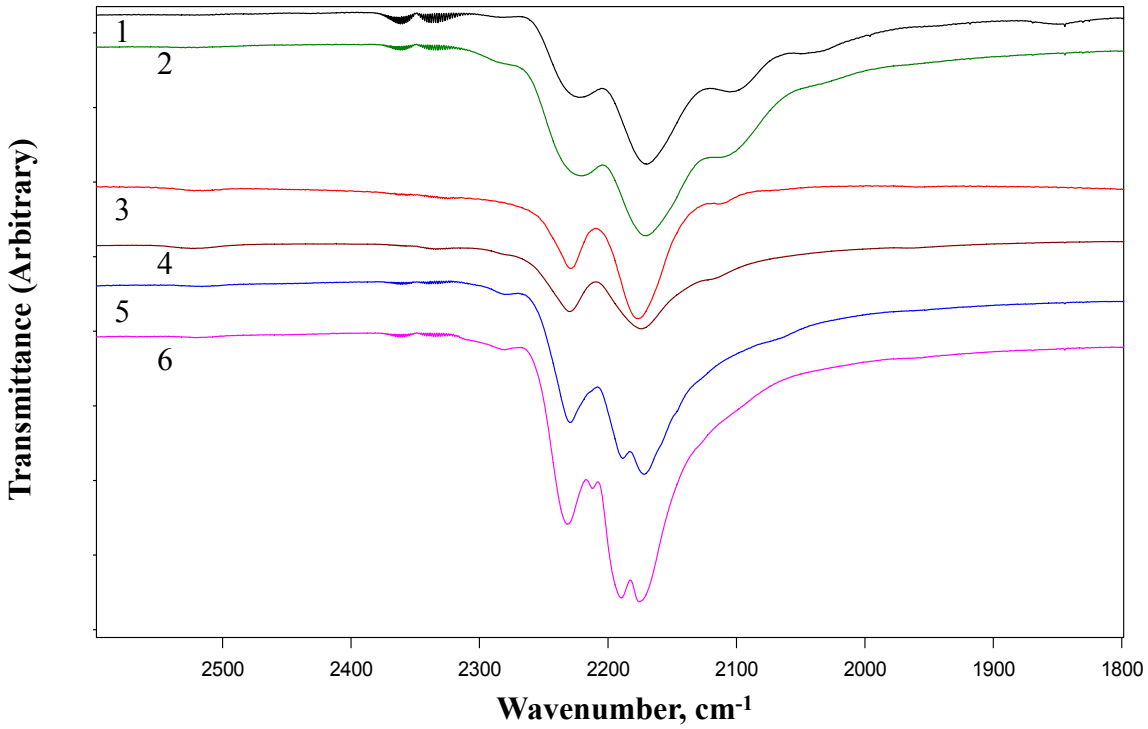

1) Film
2) Amorphous (from carbonyl)
3) $Co[C_4(CN)_8](OCMe_2)_2$
4) $Co[C_4(CN)_8]$ (dry)
5) $Co[TCNE][C_4(CN)_8]_{1/2}$
6) $Co[C_4(CN)_8](NCMe)_2$

Figure 2.5: Comparison of film **1i** with four preparations of what was expected to be $Co[TCNE]_2$ from solution.[16]

Magnetic characterization. Initial measurement attempts from the first few films failed due to lack of sample signal in the magnetometer. The Delrin holder used for the measurements had too large a signal compared to the film, and drowned out the sample's signal. For this reason, magnetic data were not collected from films **1a-c**. A change in packing technique and the use of gelatin capsules, which have a weaker diamagnetic signal compared to Delrin holders, afforded magnetic data for films **1d-f**. Beginning with film **1g**, cover slide glass was used in place of microscope slide glass to further reduce the amount of diamagnetic noise in magnetic measurements. This also allowed much more film to be packed in a gelatin capsule, as the cover slide could be broken up and packed in as opposed to the precut pieces of microscope slide.

Based on bulk data, $Co[TCNE]_2$ should be paramagnetic.[13] As such, it should follow the Curie-Weiss law:

$$\chi = \frac{C}{T - \theta} \tag{2.2}$$

where χ is the magnetic susceptibility, T is the temperature, and θ is the Weiss Constant, which is a measure of coupling within the material. The Curie constant, C, is also material-dependent, and

$$C = \frac{g^2 S(S+1)}{8} \tag{2.3}$$

where g is the Landé g-factor (which in isotropic cases ≈ 2) and S is the value of the spin on the sites that are coupled. Assuming g = 2, simplification of Equations (2.2) and (2.3) leads to an equation that gives a value for χT that only depends on the value of the spins in the material.

$$\chi T = \frac{S(S+1)}{2} \tag{2.4}$$

In a $\chi T(T)$ plot, if the sample is above its critical temperature or does not order, the data should level off and be flat as the temperature approaches room temperature. This value should agree with the tabulated value calculated from its spin values. If these films are $Co[TCNE]_2$, with the $[TCNE]^{\bullet-}$ radical anions present, Co^{2+} has a spin of 3/2 and each $[TCNE]^{\bullet-}$ will contribute a spin of 1/2, giving a room temperature χT value of 2.625 emu K/mol. If they are $Co[C_4(CN)_8]$, Co^{2+} has a spin of 3/2 and $[C_4(CN)_8]^{2-}$ has no spin. This S = 3/2 system should give a χT value of 1.875 emu K/mol at room temperature. Figure 2.6 shows the plot of $\chi T(T)$ gathered for film **1i**. This does not behave as expected for a paramagnetic system. The fact that it does not flatten out as it approaches room temperature indicates the presence of ferromagnetic impurities, which in this case would be cobalt metal impurities from the deposition.

To determine the amount of cobalt impurity in the films, the magnetization of the film, M, was measured as a function of the applied field, H. A plot is then built with χ (M/H) on the y-axis and $1/H$ on the x-axis. This plot has a linear region at high field (low

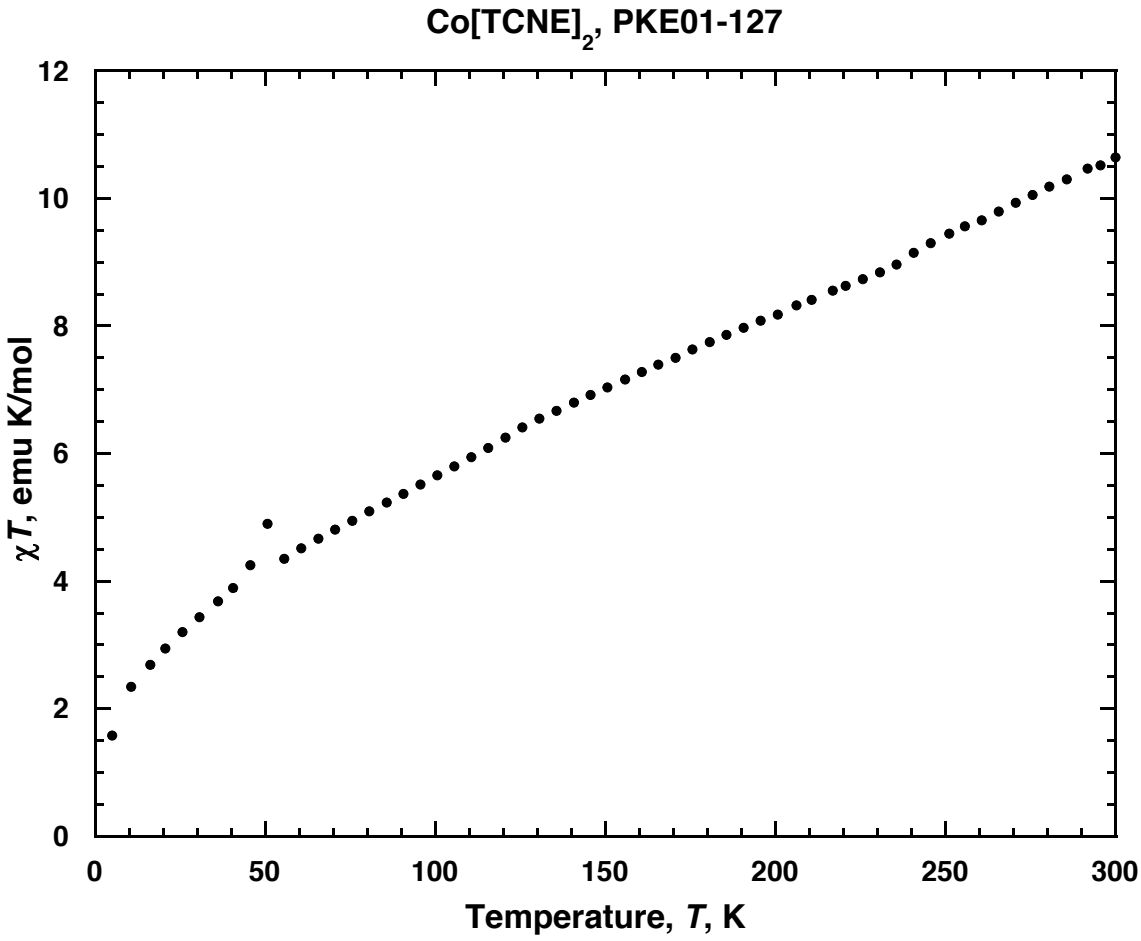

Figure 2.6: $\chi T(T)$ for film **1i**. The increasing slope of χT at room temperature indicates the presence of ferromagnetic impurities, in this case unreacted cobalt from the deposition.

$1/H$) which can be fit to find the slope using a least squares method. The plot, known as a Honda plot, for the high field region of this measurement is shown in Figure 2.7. In order to find the amount of impurities, the following formula is used:

$$C_{Co} = \frac{m}{163} \text{ x}10^6 \qquad (2.5)$$

where C_{Co} is the concentration of cobalt impurities in parts per million (ppm), m is the slope of the line, and 163 is a factor based on the number of Bohr magnetons per gram of cobalt.[20] Using Equation (2.5), the data in Figure 2.7 gives an impurity concentration of 834 ppm. This is not unexpected, as it is expected that some sublimed $Co_2(CO)_8$ does not react with TCNE, but instead deposits as metallic cobalt on the film. However, when this amount of cobalt was taken into account in the data workup, it overcorrected and gave a negative $\chi T(T)$ value. Manually adjusted, the $\chi T(T)$ plot levels off for a value of 475 ppm cobalt. This is shown in Figure 2.8.

A plot of $1/\chi(T)$ also yields important information about a magnetic material. According to the Curie-Weiss Law, such a plot for a paramagnetic material should be linear with a slope of $1/C$ and an x-intercept at $T = \theta$. Magnetic ordering will change the shape of this plot below the critical temperature (for ordering materials, θ in the Curie-Weiss law is replaced by T_c), but above T_c, the data should be linear. As can be seen in Figure 2.9, the plot of $1/\chi$ vs. T is not linear. When corrected with 475 ppm of cobalt

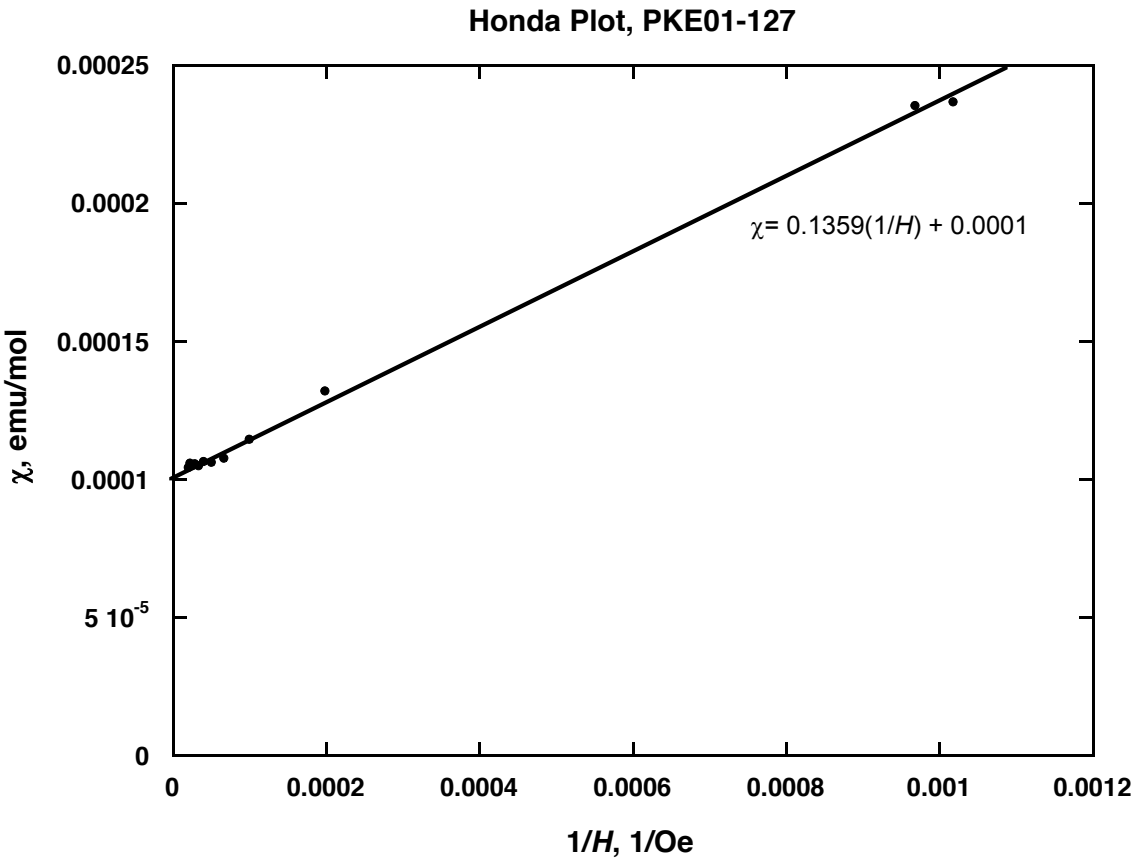

Figure 2.7: Honda plot determination of cobalt impurity concentration in film **1i**. The slope of the line in the high field region (low 1/*H*) can be used to determine the parts per million of cobalt in the film.

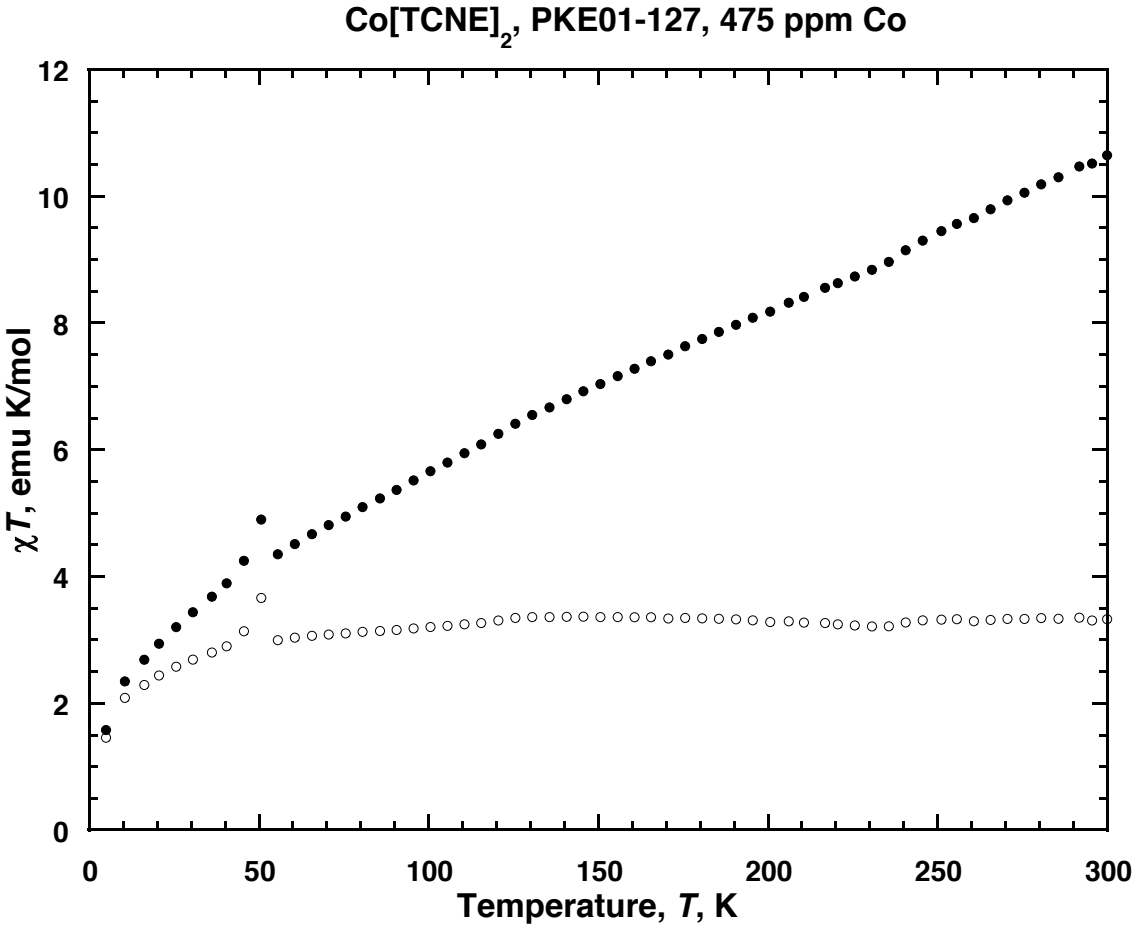

Figure 2.8: $\chi T(T)$ for film **1i**, both uncorrected (solid circles) and corrected for 475 ppm cobalt impurites (hollow circles). Note how the corrected version now levels off and is flat at room temperature.

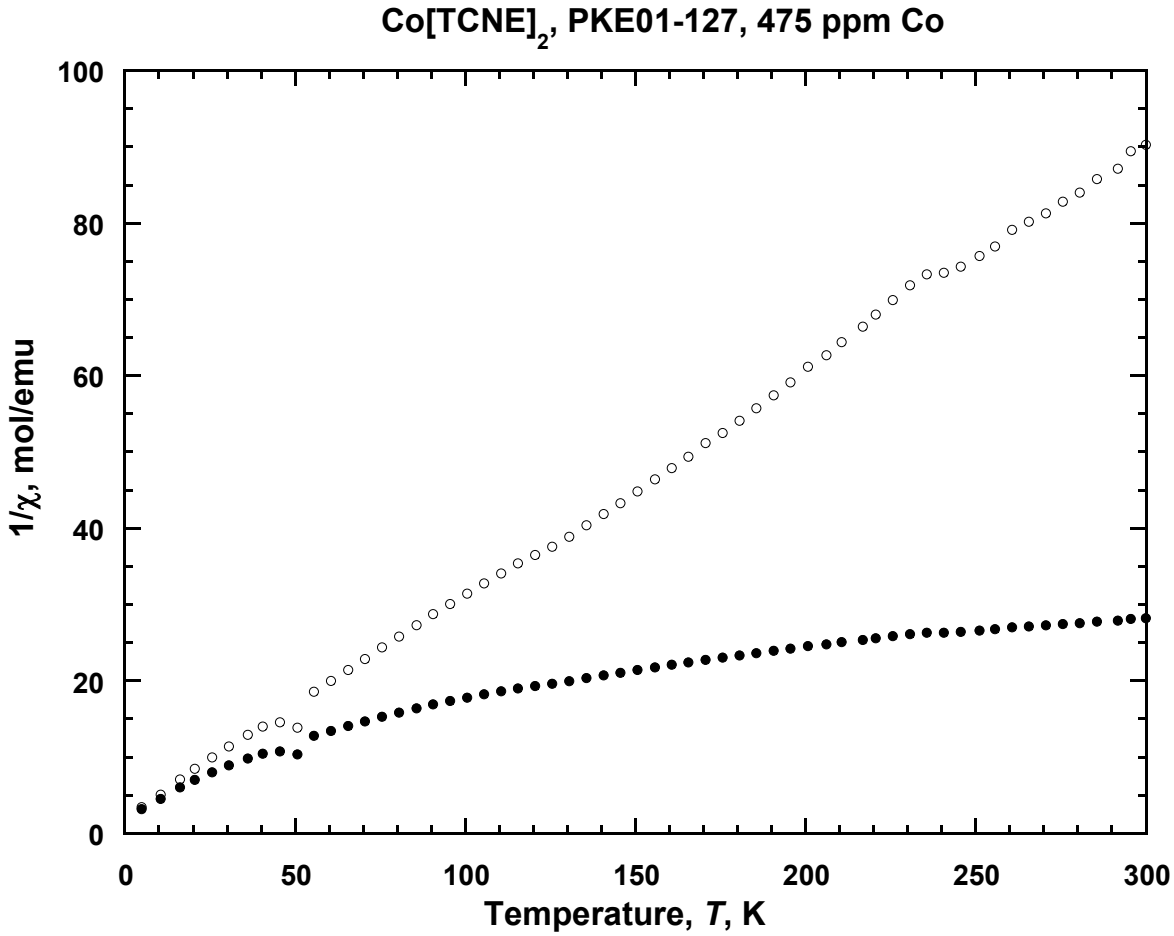

Figure 2.9: $1/\chi$ vs. T for film **1i**, both uncorrected (solid circles) and corrected for 475 ppm cobalt impurites (hollow circles). The corrected version is now linear and can be extrapolated to its x-intercept according to the Curie-Weiss law.

again, however, the plot becomes linear, with an *x*-intercept (the θ value) of -5.2 K. A negative value of θ indicates antiferromagnetic coupling.

These results, corrected for cobalt impurities, show a very strong paramagnetic trend with no indication of magnetic ordering. These data agree well with bulk data available for $Co[TCNE]_2$.

Overview of results. Structural characterization and infrared characterization by another group member of samples prepared from solution have shown evidence these films could be $Co[C_4(CN)_8]$, not $Co[TCNE]_2$. Further research is needed to confirm what the resulting structure of these films is. Regardless, thin-films of $Co[TCNE]_2$ have been made and positively identified by comparing the IR spectra of the film to its bulk counterpart. No magnetic ordering is evident in these films at the temperatures tested (5-300 K), indicating that $Co[TCNE]_2$ is paramagnetic in this range. Furthermore, data suggest antiferromagnetic coupling based on the $1/\chi(T)$ *x*-intercept value of -5.2 K. Unreacted cobalt deposited on the film in varying concentrations film-to-film, but it was possible to adjust the magnetic data to correct for these impurities by employing a Honda plot.

$V[TCNE]_2$

$V[TCNE]_2$ has been made and extensively characterized as both a bulk material and as a thin-film. The motivation for depositing $V[TCNE]_2$ thin-films for this project was simply to establish that the apparatus could reproduce past results and to establish a baseline for mixed-metal depositions involving vanadium.

Experimental

Starting materials. Vanadium carbonyl, $V(CO)_6$, was prepared from dry orthophosphoric acid, H_3PO_4, and tetraethylammonium vanadiumcarbonyl, $[Et_4N][V(CO)_6]$, according to the literature prep and in the apparatus shown in Figure 2.10.[17] 6.0 g of $[Et_4N][V(CO)_6]$ mixed with 40 g of H_3PO_4 yielded 1.5 g of $V(CO)_6$. TCNE was prepared by the same sublimation process described previously.

Chemical vapor deposition. The CVD process for $V[TCNE]_2$ is very similar to that for $Co[TCNE]_2$. The parameters are listed in Table 2.2. For films **2a** and **2b**, no magnetic data were collected, and only a KBr pellet was included to collect infrared data. Film **2c** was deposited solely on a cover slide with the intention of collecting magnetic data.

Characterization. Infrared data were collected the same as the $Co[TCNE]_2$ films. Magnetic data were collected on the same MPMS 5T SQUID magnetometer, but the temperature range was from 10-400 K, as the T_c was expected to be above room temperature.

Results and Discussion

Infrared spectroscopy. The IR spectra of the two $V[TCNE]_2$ films for which data were collected, films **2a** and **2b**, are shown in Figure 2.11. The slight variations in peak position of these two films can probably be attributed to slight differences in the molecular orientation as a consequence of different deposition parameters, as film **2a** was deposited with the TNCE at 50 ºC and the carbonyl at 10 ºC, whereas film **2b** was

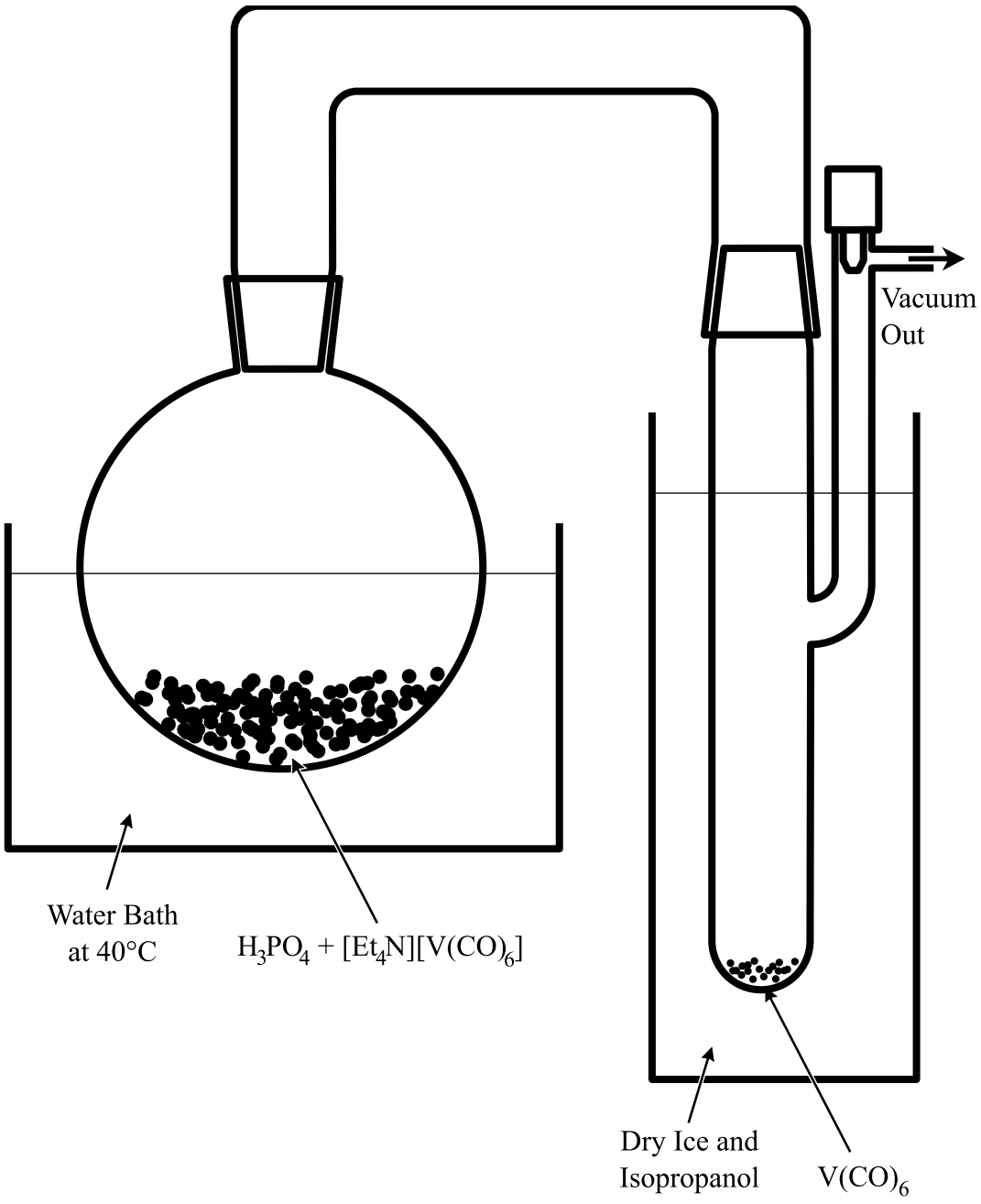

Figure 2.10: The apparatus used to produce $V(CO)_6$.[17]

Table 2.2
Deposition parameters for $V[TCNE]_2$ films.

Film	Notebook Number	Temperature of TCNE* (ºC)	Temperature of $V(CO)_6$* (ºC)	Flow Rate over TCNE‡ (SCCM)	Flow Rate over $V(CO)_6$‡ (SCCM)
2a	PKE01-101	50	10	150	100
2b	PKE01-105	55	19	150	100
2c	PKE01-147	45	17	120	100

* ±3 ºC
‡ ±5 SCCM

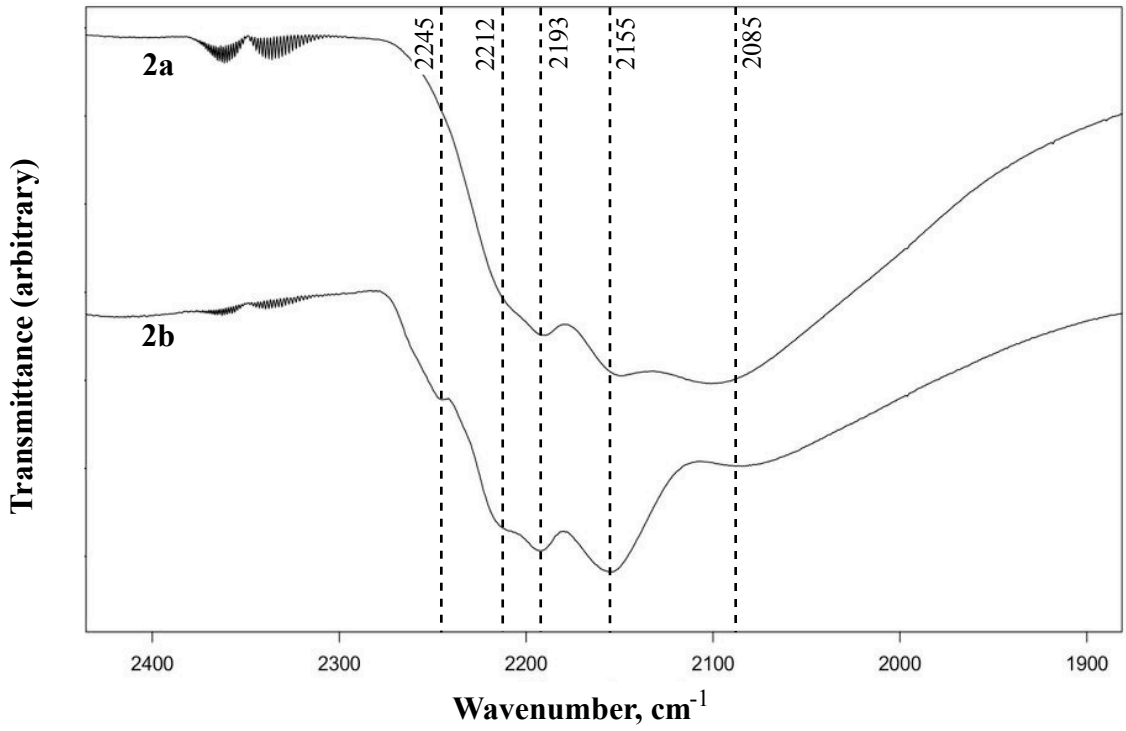

Figure 2.11: Infrared spectra of both $V[TCNE]_2$ films. Dotted lines are guides for the eye.

deposited with the TCNE at 55 ºC and the carbonyl at 19 ºC. Nevertheless, the spectra show the same number of peaks with varying intensities, and both fall in the expected range of $V[TCNE]_2$ established in the bulk phase displayed in Figure 1.6.

Magnetic data. Only one set of magnetic data was collected for a $V[TCNE]_2$ thin-film from this apparatus, for film **2c**. The magnetization, M, versus the temperature, T, is displayed in Figure 2.12. This film exhibits magnetic ordering, but not at the expected value of 350 K. On an $M(T)$ plot, the T_c of a material can be estimated by extrapolating the most linear portion of the curve as the curve approaches $M = 0$. Applying this method to film **2c**, the estimated T_c for this film is ~275 K. Again, it is unclear why such a deviation from expectation would occur, but it would have to do with differences in how the film deposited on the glass substrate.

Conclusions

Both $V[TCNE]_2$ and $Co[TCNE]_2$ films have been made. The $Co[TCNE]_2$ film, instead of having the expected structure $Co[TCNE]_2$, exhibits characteristics in the IR and magnetically that point to it possibly being $Co[C_4(CN)_8]$, thus providing an initial explanation to its paramagnetism. The $Co[TCNE]_2$ films have been further corrected to account for the presence of ferromagnetic impurities, in this case unreacted cobalt metal that deposits on top of the film.

The $V[TCNE]_2$ films have the same IR characteristics as their bulk counterparts. The one film characterized magnetically shows ordering up to a T_c of ~275 K, lower than the expected value of >350 K, but it can be confidently assumed that adjustment of

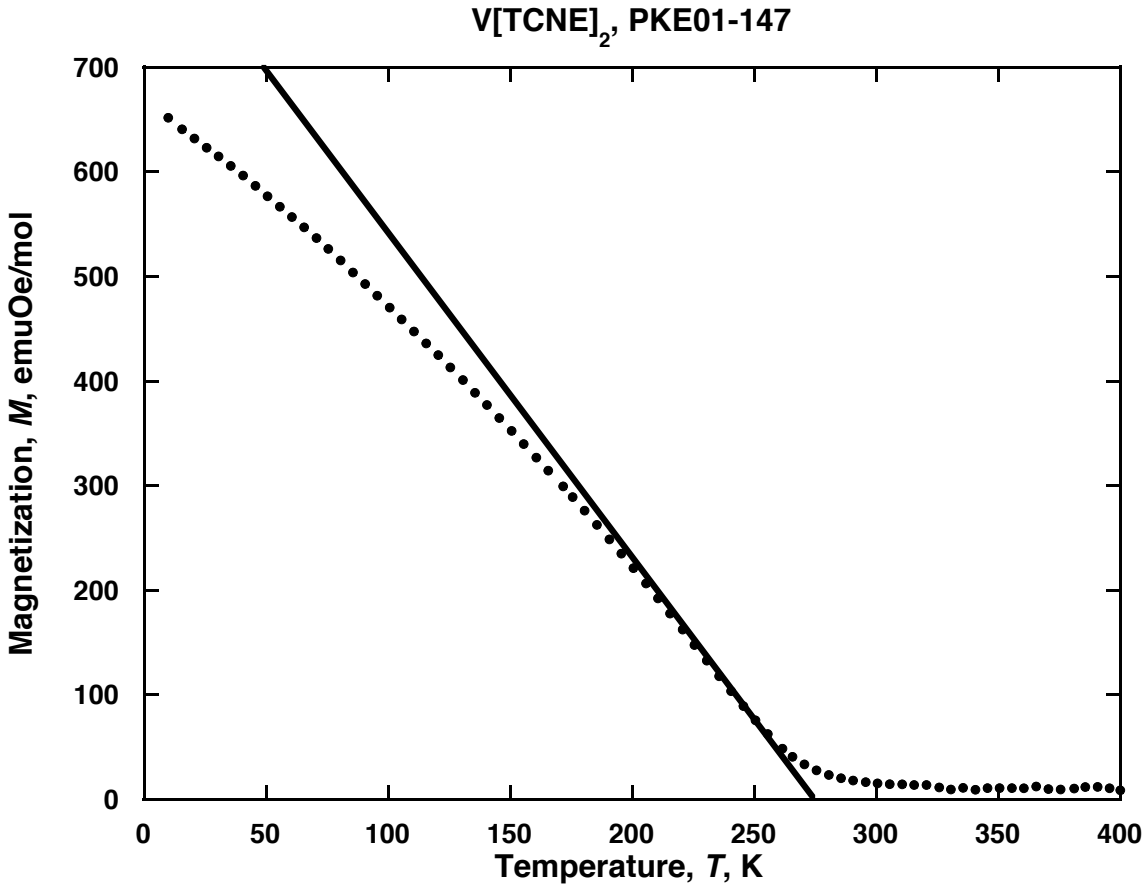

Figure 2.12: $M(T)$ plot of film **2c**. Extrapolation of the most linear region before it levels off (added line) give an estimate for T_c. 275 K is an uncharacteristically low T_c for $V[TCNE]_2$.

deposition parameters would produce films with ordering temperatures equal to that of the bulk material and thin-films produced in the past.

CHAPTER 3

MIXED-METAL TCNE FILMS

Once the chemical vapor deposition apparatus was set up and the procedure for making single-metal TCNE films was established, the focus of this research turned to a novel material, a mixed-metal film of composition $V_xCo_{1-x}[TCNE]_2$.

$V_xCo_{1-x}[TCNE]_2$

Experimental

Starting materials. The starting materials for these films are the same as those described in Chapter 2. Both TCNE and $Co_2(CO)_8$ were purified from commercially available sources by sublimation. $V(CO)_6$ was prepared by reaction of $[Et_4N][V(CO)_6]$ and phosphoric acid, H_3PO_4 as described previously.[17]

Chemical vapor deposition apparatus. The majority of the glassware used in the CVD apparatus for the single-metal TCNE films were used for the mixed-metal TCNE films. The major difference, however, was the necessity to facilitate the introduction of two metal carbonyls in vapor phase into the center of the chamber at the same time. Governed by the availability of only one peltier unit for cooling the carbonyls, the new design arrived upon for the carbonyl tube is shown in Figure 3.1.

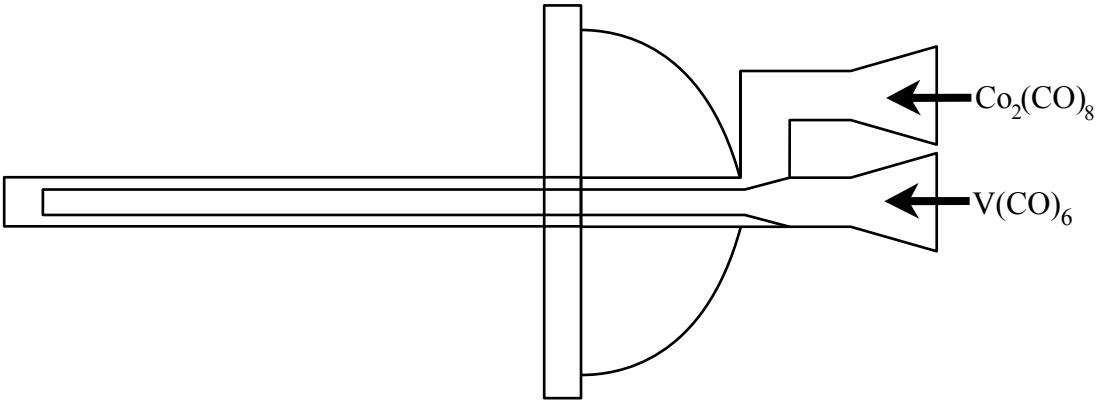

Figure 3.1: New tube for the introduction of carbonyls into the deposition zone of the CVD apparatus.

This new tube consists of an outer tube the same diameter as the original tube, but down the center of this outer tube is a smaller tube. Each tube has an input isolated from the other, and the two vapor streams meet less than half an inch before the end of the tube.

Furthermore, it was necessary to keep the $Co_2(CO)_8$ and the $V(CO)_6$ separated as long as possible because, in experimenting with having both carbonyls in the same holder (in the single-metal film setup), the metals both mirrored out significantly before flowing down the tube, and no film deposited. Further testing was performed to see if the carbonyls preferred the outer tube or the inner tube. The $V(CO)_6$ performed the same in either tube, but when the $Co_2(CO)_8$ was placed in the inner tube it mirrored out before the end of the tube and no film resulted. Thus, the $Co_2(CO)_8$ was always placed to go down the outer tube, and the $V(CO)_6$ down the inner tube, as designated in Figure 3.1.

A minor modification to the carbonyl boats was necessary, as the carbonyl holder for the single-metal TCNE films was large enough that two could not sit side-by-side in the silicon oil bath on the peltier unit. For this reason, two holders were made that were small enough to sit side-by-side and allow both carbonyls to be cooled to an appropriate temperature.

Chemical vapor deposition. With the ideal temperature for the TCNE set (45 ºC) to minimize waste, and the ideal flow rates for the TCNE (120 SCCM) and carbonyls (100 SCCM), the main variable to determine was the ideal temperature for the carbonyls. In the single-film depositions, the $Co_2(CO)_8$ was kept at 10 ºC and the $V(CO)_6$ at 17 ºC. As the goal of this project was to create a film with as high a coercive field as possible, which in bulk samples occurs at $x = 0.3$, it was decided to maintain both carbonyls at 17

ºC. This should allow for more $Co_2(CO)_8$ to evolve and hopefully shift the composition of the films towards $V_{0.3}Co_{0.7}[TCNE]_2$. A few other temperatures were used to compare, but 17 ºC was used most of the time. All mixed-metal TCNE films were deposited on cover glass slide. The deposition parameters for all of the mixed-films attempted are in Table 3.1.

Characterization. The instrumentation for infrared and magnetic characterization are the same as previously described in Chapter 2. Two main sets of data were run for each mixed-metal TCNE film: susceptibility versus temperature from 10-400 K and hysteresis at 5 K up to 5 tesla (T).

In addition to infrared spectroscopy and magnet data, two more tools were used to characterize these films. A scanning electron microscope (SEM) (Hitachi 5-3000N in the Materials Characterization Lab, Materials Science and Engineering Department) was used to observe the surface of the films, checking for uniformity and other observable features. An attachment on the SEM (EDAX PV7746) was used for energy dispersive x-ray spectroscopy (EDS), which gives information about the composition of a material and was used specifically to detect the ratio of vanadium to cobalt in these films.

Results and Discussion

Composition of films. The amount of vanadium and cobalt varied greatly from film to film. Initially, the KBr pellets used for IR spectra were the only samples analyzed by EDS, but it was discovered that the films did not deposit uniformly across both substrates, and the average composition on the KBr could vary greatly from the average

Table 3.1
Deposition parameters for $V_xCo_{1-x}[TCNE]_2$ films.

Film	Notebook Number	Temperature of TCNE* (ºC)	Temperature of Carbonyls* (ºC)	Flow Rate over TCNE‡ (SCCM)	Flow Rate over Carbonyls‡ (SCCM)
3a	PKE01-117	45	17	120	100
3b	PKE01-119	45	17	120	100
3c	PKE01-121	45	17	120	100
3d	PKE01-125	45	17	120	100
3e	PKE01-129	45	13	120	100
3f	PKE01-131	45	26	120	100
3g	PKE01-133	45	10	120	100
3h	PKE01-135	45	15	120	100
3i	PKE01-137	45	17	120	100
3j	PKE01-143	45	17	120	100
3k	PKE01-145	45	10	120	100

* ±3 ºC
‡ ±5 SCCM

composition on the cover glass. The amounts of vanadium and cobalt (represented as percentage of total metal content) present in the films are reported in Table 3.2. There are three main areas of variation for compositions in these films: different compositions between two samples, different composition between the KBr pellet and cover glass of the same sample, and a composition gradient within the film on a single substrate.

Regarding the differences in composition from sample to sample, no ready explanation can be proposed with the data present. Most of the films were deposited under the same conditions, yet they show a large spread in compositions. This can only be attributed to unexpected variables that have not been accounted for, such as the exact position of the substrates in relation to the input tubes, exact time run, or the surface area of starting material crystals (affecting sublimation rates). Future work on this project should attempt to duplicate conditions from sample to sample as precisely as possible.

The simplest explanation for the variation in composition across a substrate has to do with geometry. A cross section of the deposition chamber at the center, where the substrates are placed, is shown in Figure 3.2. The cover slide is longer than the side of the square substrate holder is wide, and is therefore sitting at an angle. The KBr pellet is small enough to sit flat against the glass of the substrate holder. The metal carbonyls come out at the center of the tube, and both presumably react with TCNE to form the resulting films. If one of the carbonyls is heavier, more volatile, or more reactive than the other, it is feasible that a composition gradient would arise on a substrate solely based on this factor. A map of values of x, the vanadium fraction in $V_xCo_{1-x}[TCNE]_2$ on the KBr pellet of film **3h,** is shown in Figure 3.3. There is a clear gradient from bottom to top

Table 3.2
Composition of $V_xCo_{1-x}[TCNE]_2$ films measured by EDS.

Film	% of V and Co in $V_xCo_{1-x}[TCNE]_2$ on KBr	Error*	% of V and Co in $V_xCo_{1-x}[TCNE]_2$ on Glass	Error*
3a	V: 54 Co: 46	± 3	V: 32 Co: 68	± 5
3b	V: 83 Co: 17	± 1	V: 36 Co: 64	± 5
3c	No Data Available	--	V: 72 Co: 28	± 5
3d	V: 86 Co: 14	± 3	V: 36 Co: 64	± 12
3e	No Data Available	--	V: 56 Co: 44	±10
3f	No Film	--	No Film	--
3g	No Film	--	No Film	--
3h	V: 56 Co: 44	± 14	No Data Available	--
3i	V: 76 Co: 24	± 4	V: 50 Co: 50	± 22
3j	V: 52 Co: 48	± 1	V: 45 Co: 55	± 11
3k	No Data Available	--	V: 53 Co: 47	± 16

***** Error reported as one standard deviation of the available data.

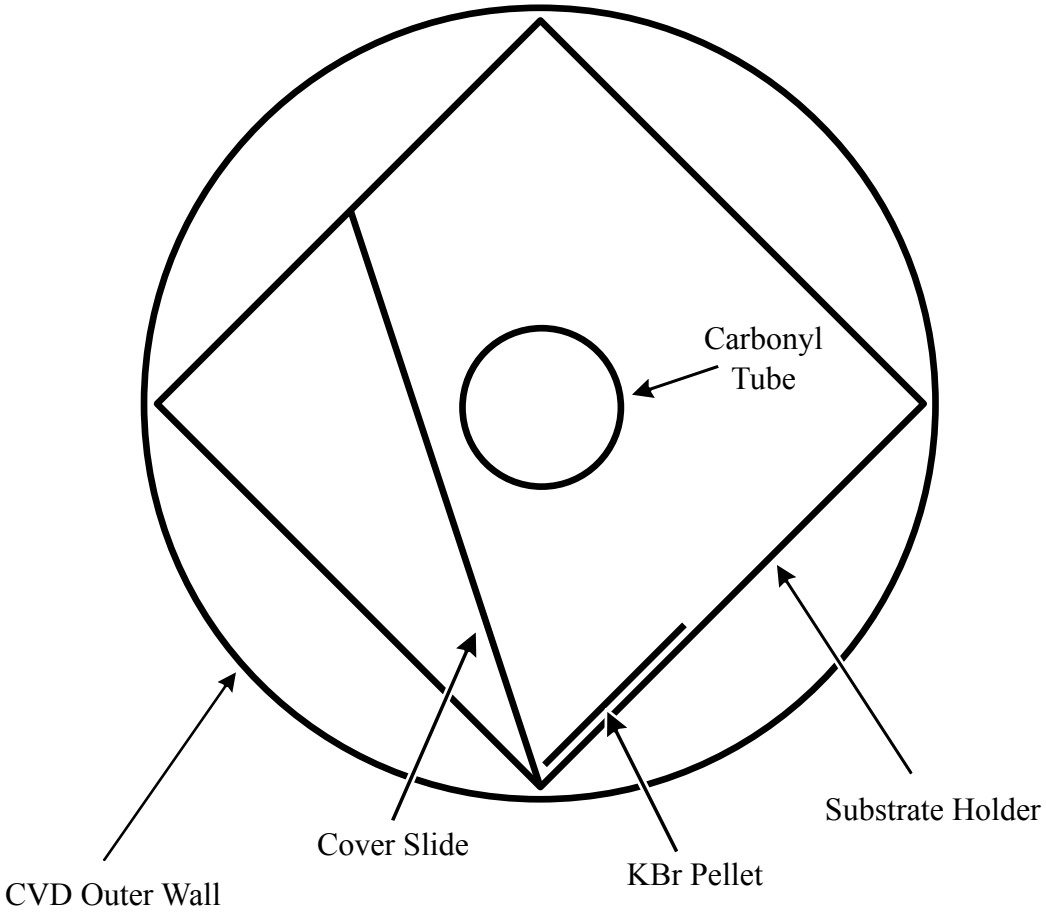

Figure 3.2: Cross section of the CVD chamber at the midpoint.

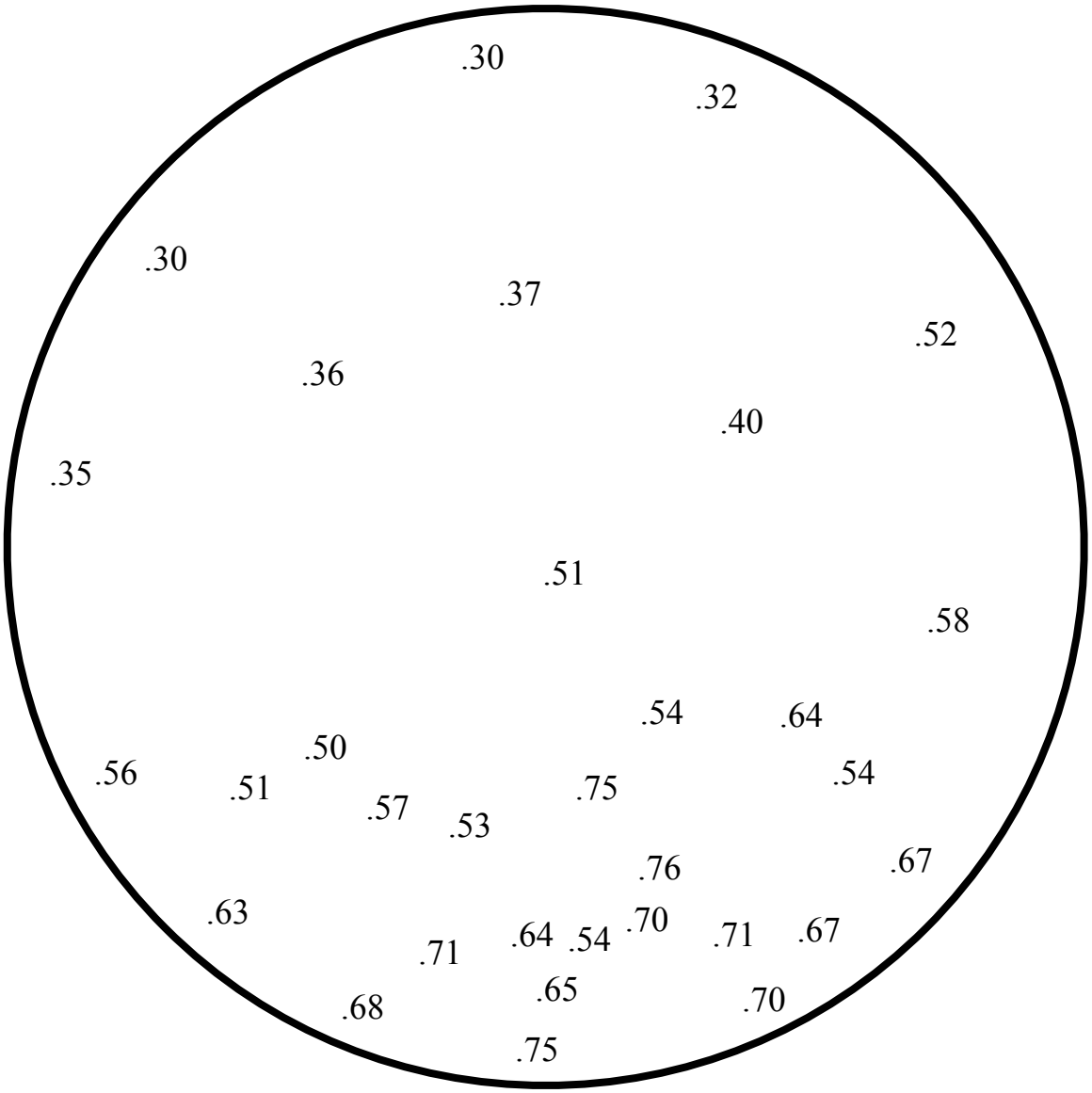

Figure 3.3: Compositin map of film **3h** measured by EDS. Values are fraction of vanadium, *x*, in $V_xCo_{1-x}[TCNE]_2$.

which could be a result of geometry. Figure 3.4 is a photograph where regions of different composition are visible by eye on film **3b**.

This effect may also play a role in the difference in composition between the cover glass and the KBr pellet, as the glass is much closer to where the carbonyls enter the reaction zone. This would account for the fact that the compositions on glass exhibit a wider spread than on KBr (indicated by the larger standard deviations in the data set).

One trend established in films with data for both KBr and glass compositions is that the KBr always has a higher vanadium concentration than the corresponding cover slide. This may also be a geometric factor, but there may be another factor in this trend. The metals may show preferential deposition, favoring one substrate to the other. It is impossible to tell if these composition differences are from one factor or the other, or a combination of the two, but these are the most apparent theories at the time.

Infrared spectroscopy. All of the IR spectra of the mixed-metal TCNE films (**3f** and **3g** not included because no film resulted from those depositions) are shown in Figure 3.5. All of the spectra are similar in the C≡N region (between 2000 cm^{-1} and 2300 cm^{-1}). In the region between 2000 cm^{-1} and 2100 cm^{-1}, the first half of the films exhibit an unidentified broad peak that is more intense than the peaks of interest, but this trend disappears in the second half of the films. As of now, no explanation has been offered for this feature.

The interest in infrared data for these films is in comparison with pure $V[TCNE]_2$ and $Co[TCNE]_2$. As a reminder, Figure 1.6 shows the composition gradient for the bulk materials. The IR's of four films, **1c**, **2b**, **3e**, and **3h**, starting with pure $V[TCNE]_2$ on top

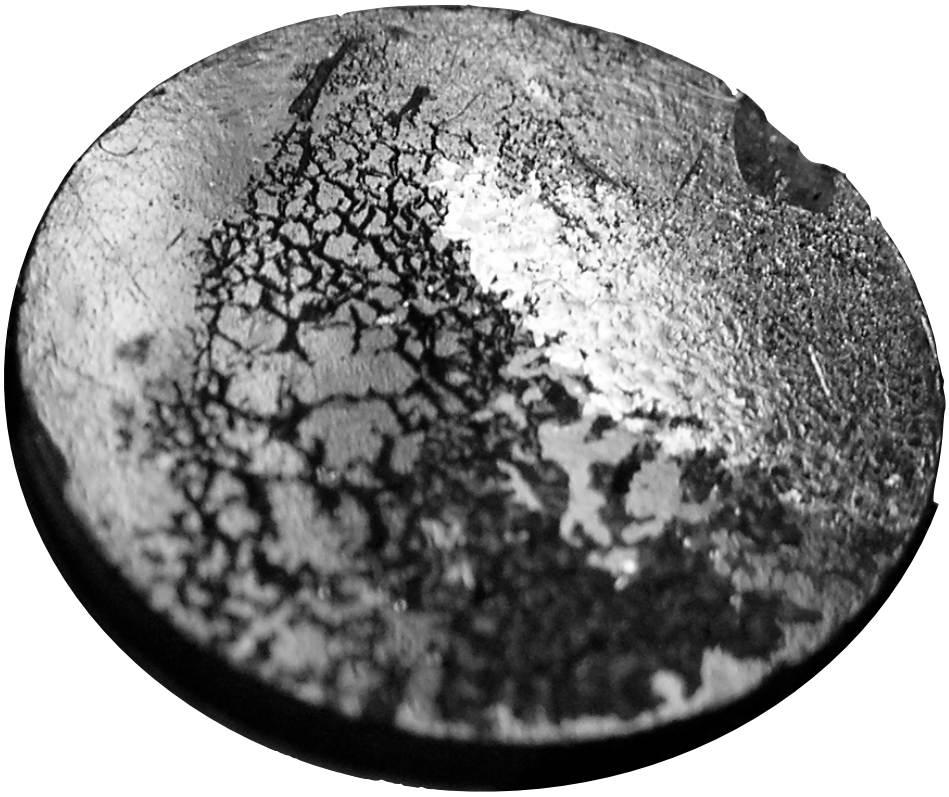

Figure 3.4: Photograph of film **3b** showing regions of different composition visible with no magnification.

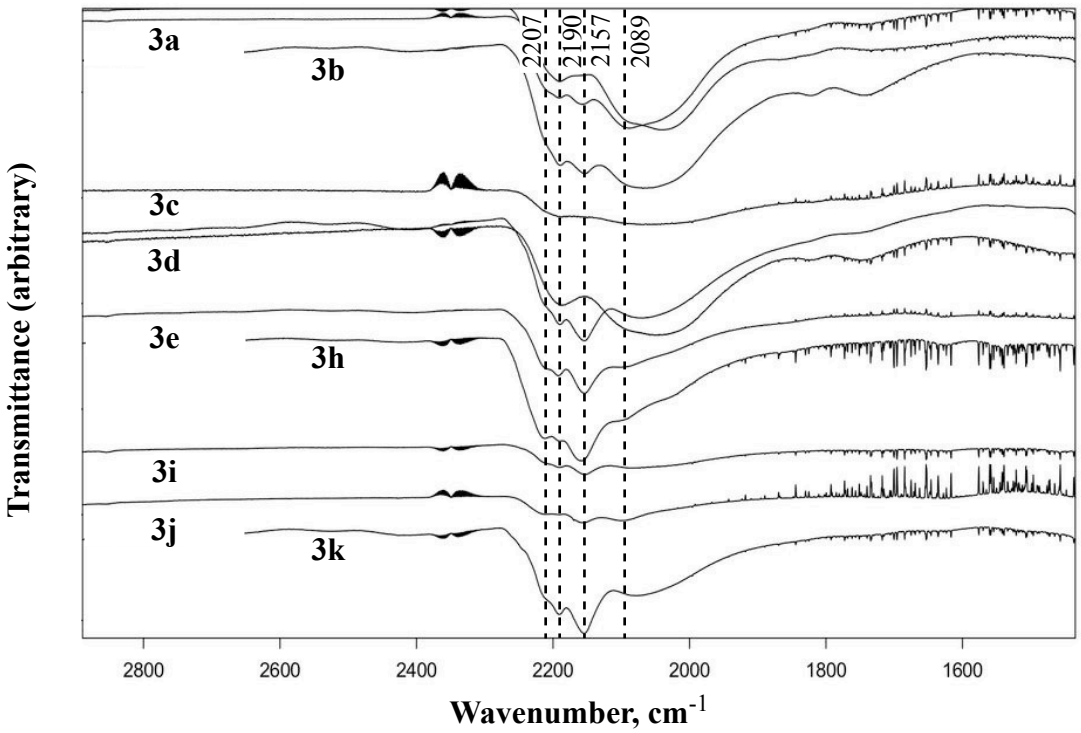

Figure 3.5: Infrared spectra of mixed-metal $V_xCo_{1-x}[TCNE]_2$ films. Dotted lines are guides for the eye.

and moving to pure $Co[TCNE]_2$ on bottom, are shown in Figure 3.6. Film **3e**, although data are not available for the composition of the KBr pellet, exhibits the beginning of a transition, with the shoulder at 2085 cm^{-1} decreasing in intensity as well as the small peak at 2245 cm^{-1} beginning to disappear. Film **3h**, with an average composition of $V_{0.56}Co_{0.44}[TCNE]_2$, shows more of the transition, with a shoulder beginning to appear at 2041 cm^{-1}, the peak at 2245 cm^{-1} disappearing completely, and the peak at 2155 cm^{-1} beginning to shift toward the main cobalt peak at 2173 cm^{-1}.

These infrared data, combined with the EDS data presented above, prove that the starting materials are reacting and films with composition $V_xCo_{1-x}[TCNE]_2$ are indeed being produced. The final piece of information needed was to look at the magnet data to see if the inclusion of cobalt increases the coercive field of these thin-films.

Magnetic characterization. Magnetic data were collected for seven of the eleven mixed-metal TCNE film deposition products. Films **3d**, **3e**, and **3h** exhibited T_c's greater than 350 K, which is expected for $V_xCo_{1-x}[TCNE]_2$. Films **3i-k** showed T_c's around 300 K, and film **3b** had a T_c of approximately 260 K. Similar to film **2c**, the reason this film's critical temperature is so low is not known. With all seven magnetically characterized thin-films ordering magnetically, one goal has been met, to make magnetic thin-films with both vanadium and cobalt present with TCNE.

The $\chi T(T)$ and $1/\chi(T)$ plots for film **3h** are shown in Figures 3.7a and 3.7b, respectively. The original $\chi T(T)$ plot had a slight positive slope above the critical temperature, which was corrected with 500 ppm cobalt. The portion of the $1/\chi(T)$ plot

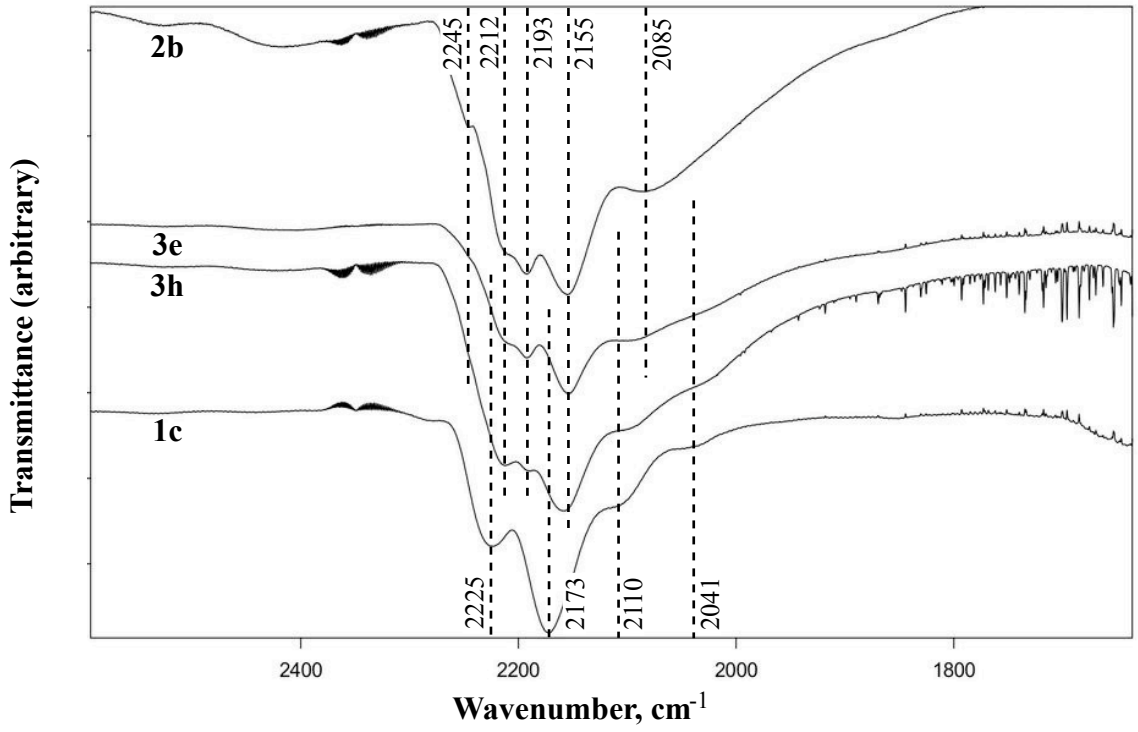

Figure 3.6: Infrared spectra comparison of $Co[TCNE]_2$, $V[TCNE]_2$, and two mixed-metal $V_xCo_{1-x}[TCNE]_2$ films. Dotted lines are guides for the eye.

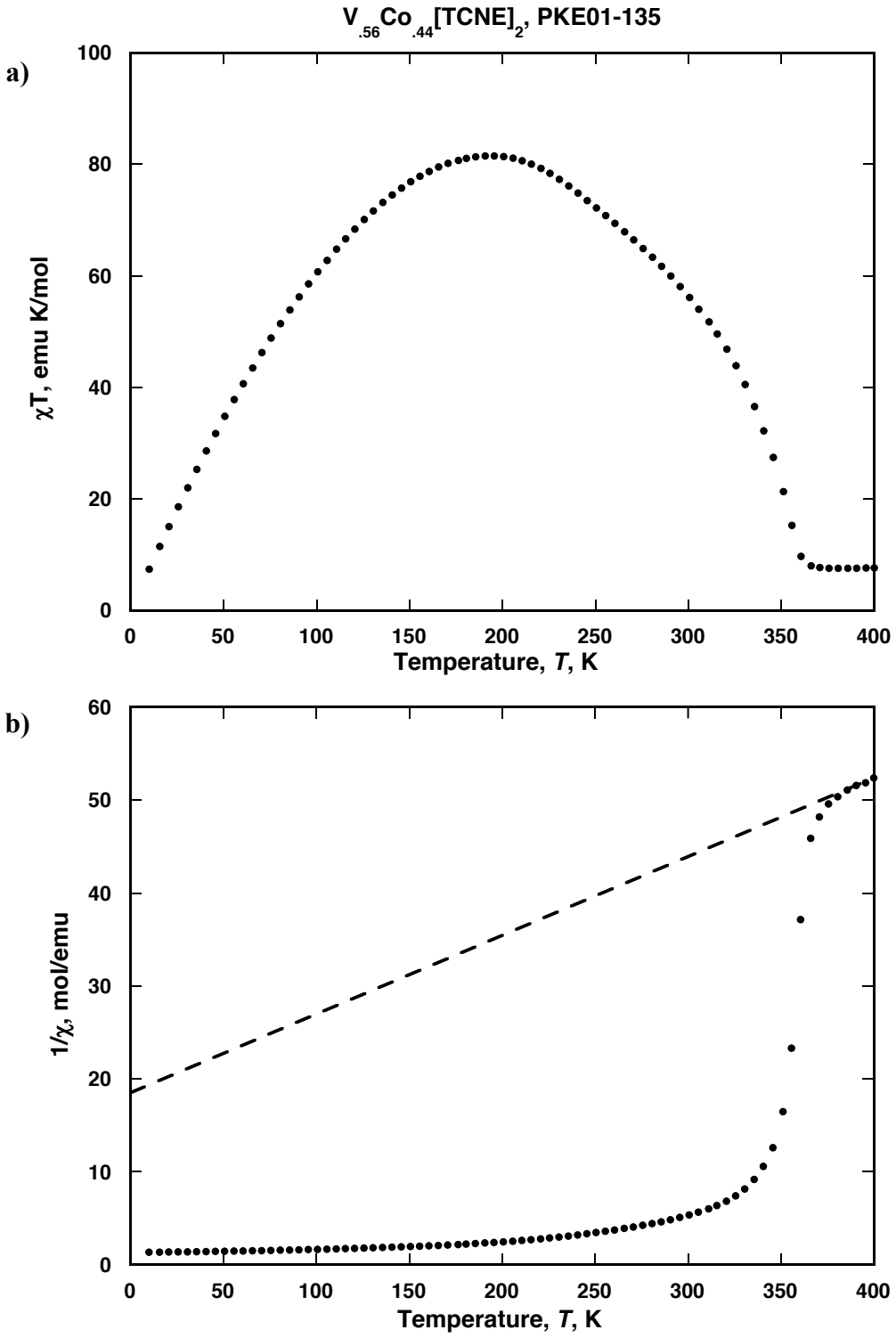

Figure 3.7: Magnetic data for film **3h**. a) $\chi T(T)$ and b) $1/\chi(T)$. The negative x-intercept in $1/\chi(T)$ indicates antiferromagnetic coupling.

above the critical temperature that begins to behave linearly can be extrapolated (the dotted line) to a negative θ value which indicates antiferromagnetic coupling.

Another interesting characteristic of these films which has carried over from the bulk material is that they decompose if heated above 350 K. Since the susceptibility needs to be measured up to 400 K to get good data, all films decomposed upon measurement. The $\chi T(T)$ of film **3d** is plotted twice in Figure 3.8, the first curve being the first time it was measured, and the second curve after being cooled and measured again. Note how in the second run, there is now a positive slope to $\chi T(T)$ at room temperature, indicating the new presence of ferromagnetic impurities, assumed to be cobalt metal from further decomposition.

The main focus of this project, though, was on hysteresis and coercive field. As a reminder, bulk $V[TCNE]_2$ has a coercive field of 7.8 Oe at 5 K. Any significant improvement on this value would be a success. Five of the magnetically characterized films had coercive fields at 5 K of 10 Oe or less. The hysteresis loop for film **3i** is shown in Figure 3.9. For the other two, films **3b** and **3d**, the hysteresis measurements were taken after the films had been exposed to 400 K temperatures. As a result, they both decomposed before the hysteresis could be measured correctly. The decomposed films showed hysteresis, however, and the results are interesting: both exhibited coercive fields above 100 Oe. The hysteresis loop of films **3b** and **3d** are shown in Figures 3.10 and 3.11, respectively. **3b** has a coercive field, H_{cr}, of ~180 Oe and **3d** of ~105 Oe.

The reason these films do not exhibit increased coercive field is not known at this time. IR data (Figures 3.6 and 1.6) indicate that there is a composition between $x = 0$ and

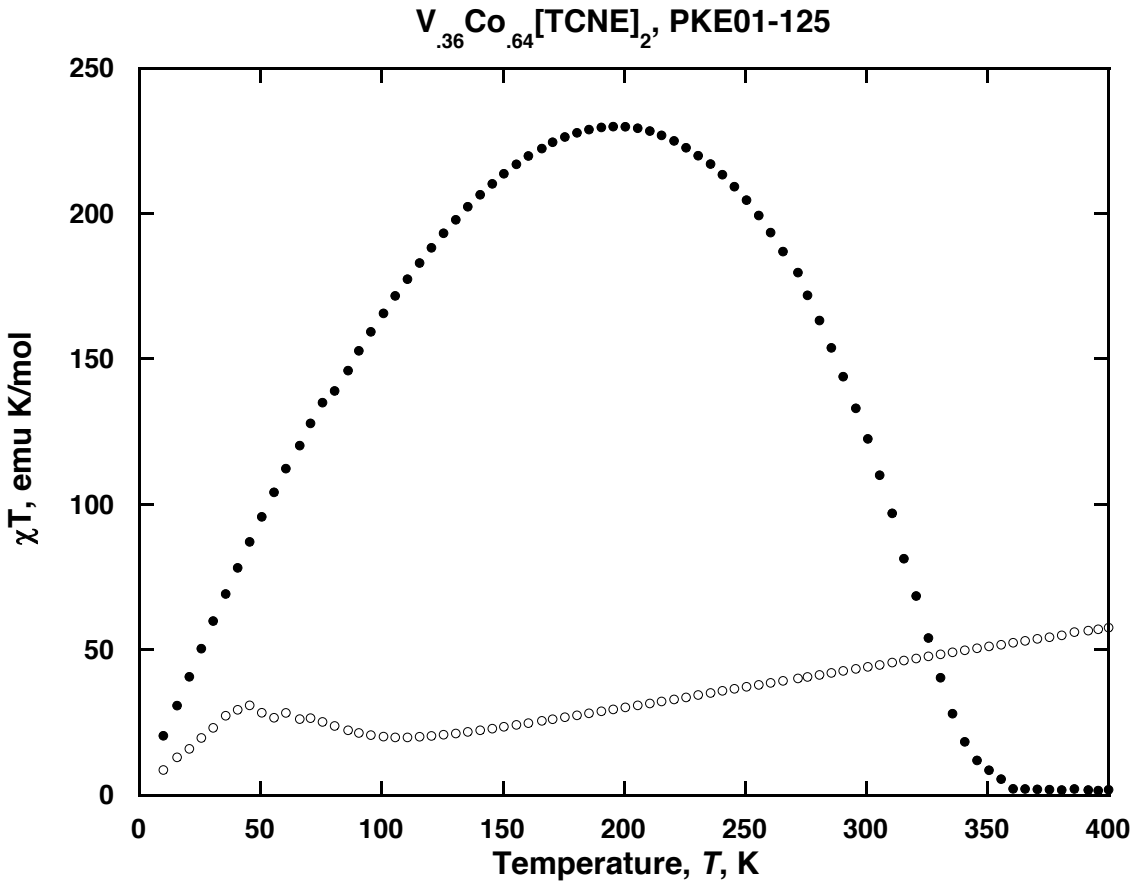

Figure 3.8: $\chi T(T)$ data for film **3d**. The first measurement (solid circles) shows magnetic ordering up to ~350 K and a flat χT above T_c. The second measurement (hollow circles) shows the film's behavior after exposure to 400 K. T_c has decreased considerably and the positive slope indicates cobalt impurities resultant from film decomposition.

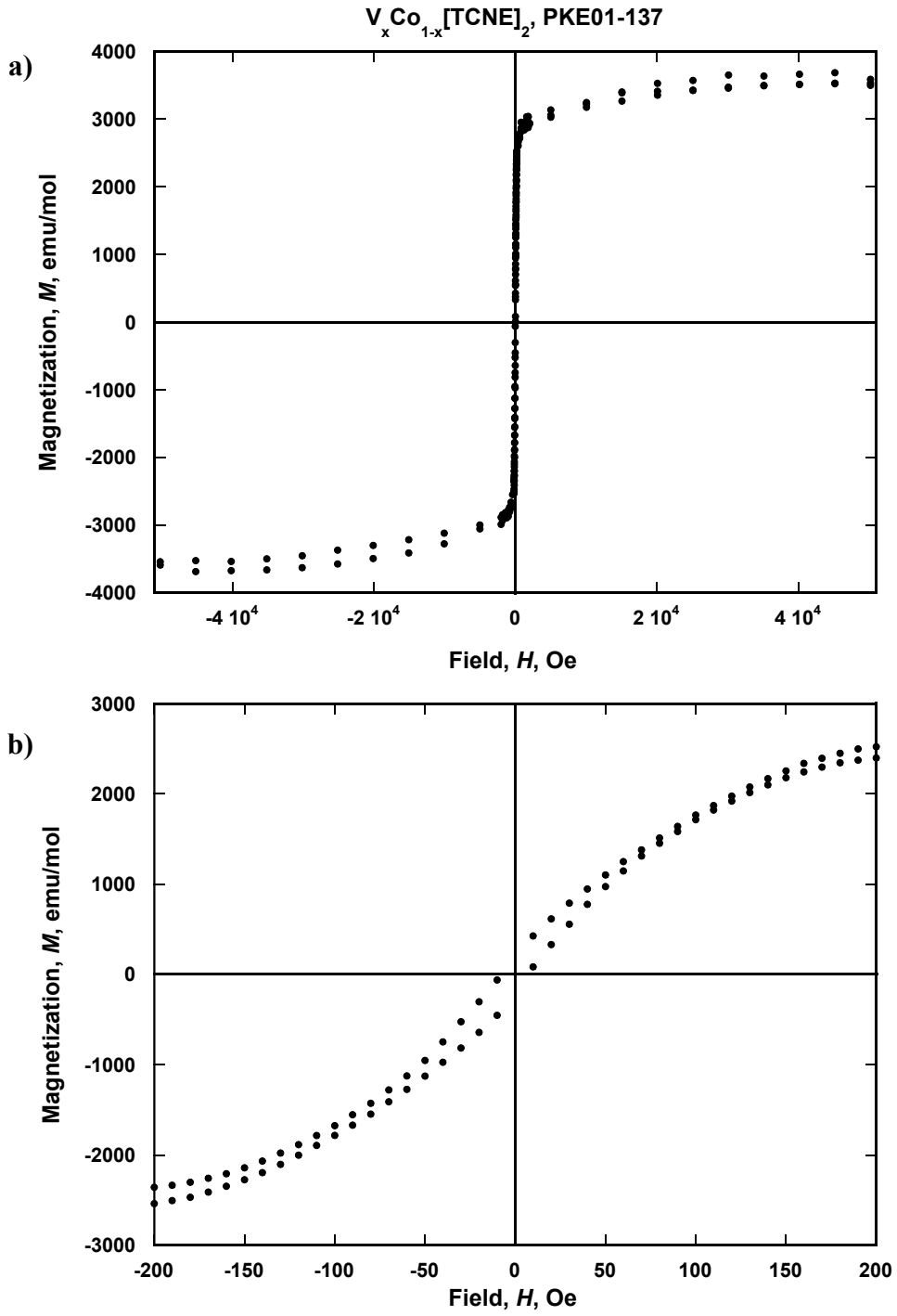

Figure 3.9: Hysteresis data at 5 K for film **3i**. a) Hysteresis loop shown to 5 T. b) Zoom on the coercive field, ~10 Oe.

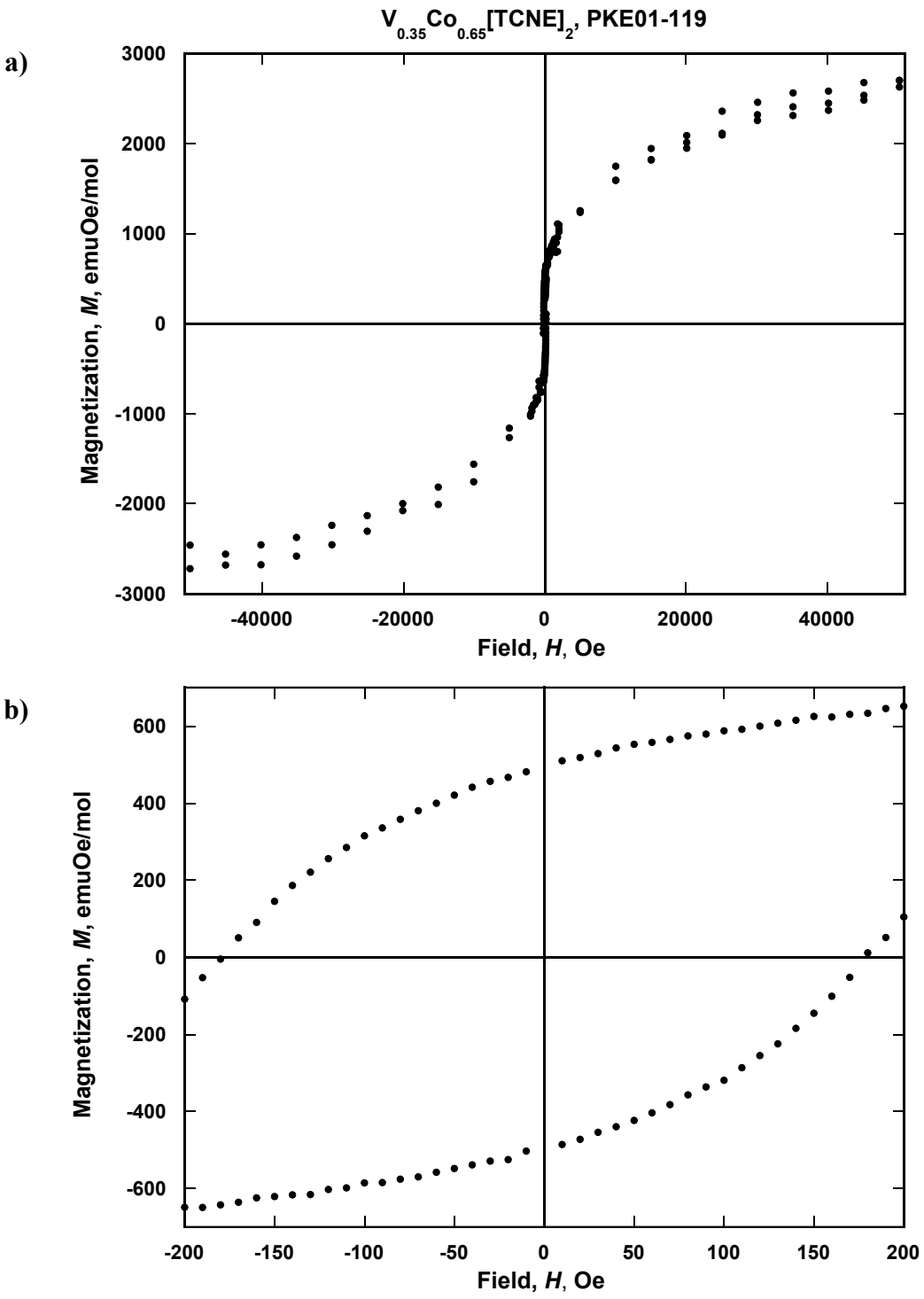

Figure 3.10: Hysteresis data at 5 K for film **3b**. a) Hysteresis loop shown to 5 T. b) Zoom on the coercive field, ~180 Oe.

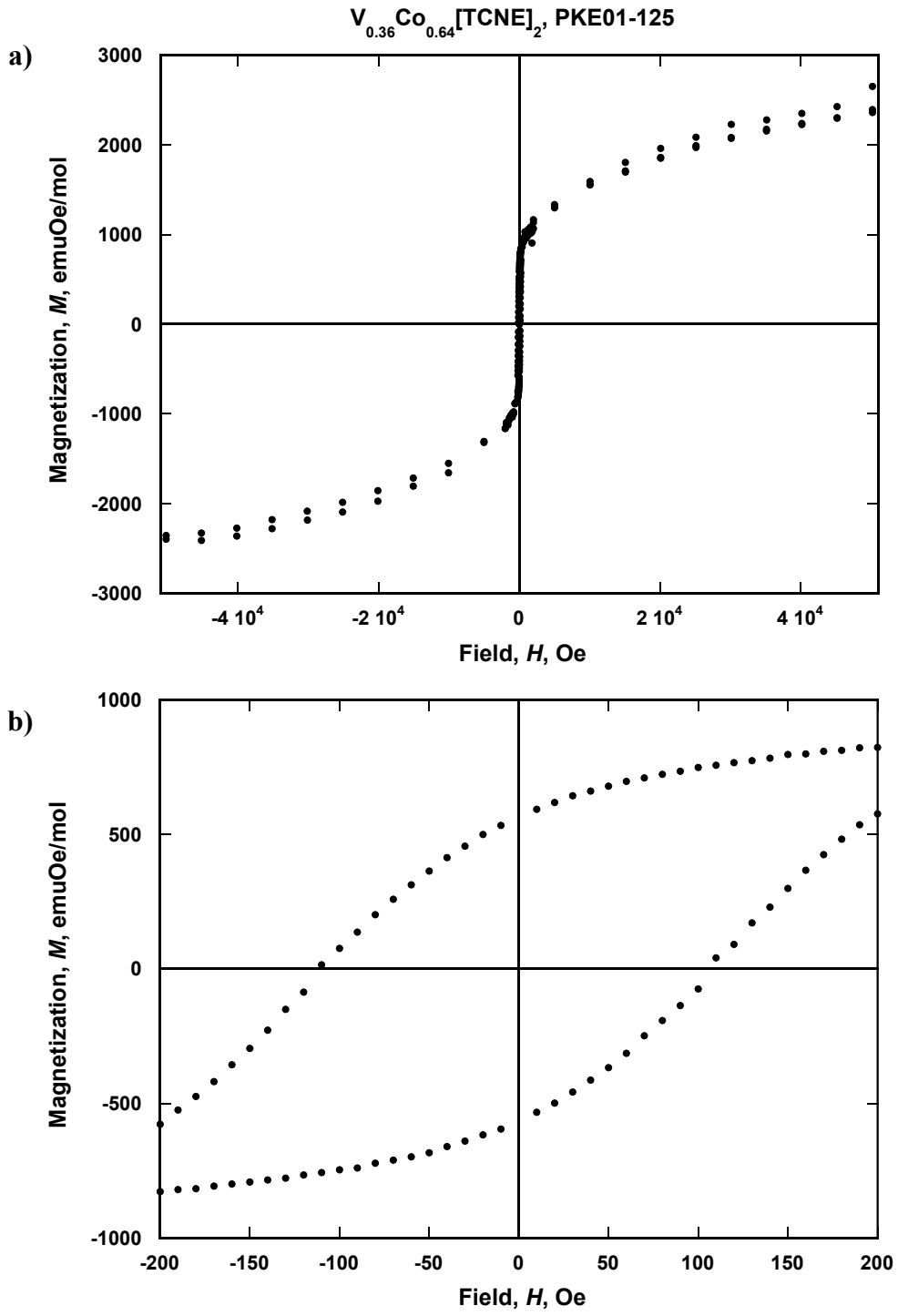

Figure 3.11: Hysteresis data at 5 K for film **3d**. a) Hysteresis loop shown to 5 T. b) Zoom on the coercive field, ~105 Oe.

x = 1 (x is the fraction of vanadium) in the mixed-metal TCNE films. This mixed composition should manifest itself with an increased coercive field as it does when this material is prepared from solution. Future research will determine if this is always the result, or if there are CVD routes that will produce a thin-film $V_xCo_{1-x}[TCNE]_2$ magnet with a greater value of coercive field.

Conclusions

A chemical vapor deposition route was designed and implemented for both single-metal ($V[TCNE]_2$ and $Co[TCNE]_2$) and mixed-metal ($V_xCo_{1-x}[TCNE]_2$) thin-films. The single-metal TCNE films behaved more or less as expected. Most importantly, the mixed-metal TCNE films deposited successfully a majority of the time. However, no increase in coercive field was measured for any of these films, regardless of composition. Further work on this project could continue exploring a CVD route to achieve a higher coercive field in these mixed-metal TCNE thin-films, creating a viable magnetic material for several potential applications.

REFERENCES

[1] M. Blackman, "The Lodestone: a Survey of the History and the Physics," *Contemp. Phys.*, **24** [4] 319-31 (1983).

[2] For an in depth overview on the development of quantum magnetic theories, see: D.C. Mattis, *The Theory of Magnetism Made Simple*, World Scientific Publishing Co. Pte. Ltd., Hackensack, NJ, 2006.

[3] D. Craik, *Magnetism: Principles and Applications*, John Wiley & Sons Ltd., West Sussex, England, 1995.

[4] G.A. Candela, L.J. Swartzendruber, J.S. Miller, and M.J Rice, "Metamagnetic Properties of One-Dimensional Decamethylferrocenium 7,7,8,8-tetracyano-p-quinodimethanide (1:1):$[Fe(\eta^5\text{-}C_5Me_5)_2]^{+\bullet}[TCNQ]^{-\bullet}$," *J. Am. Chem. Soc.*, **101** [10] 2755-56 (1979).

[5] J.S. Miller, J.C. Calabrese, H. Rommelmann, S.R. Chittipeddi, J.H. Zhang, W.M. Reiff, and A.J. Epstein, "Ferromagnetic Behavior of $[Fe(C_5Me_5)_2]^{+\bullet}[TCNE]^{-\bullet}$. Structural and Magnetic Characterization of Decamethylferrocenium Tetracyanoethenide, $[Fe(C_5Me_5)_2]^{+\bullet}[TCNE]^{+\bullet}\bullet MeCN$, and Decamethylferrocenium Pentacyanopropenide, $[Fe(C_5Me_5)_2]^{+\bullet}[C_3(CN)_5]^{-}$," *J. Am. Chem. Soc.*, **109** [3] 769-81 (1987).

[6] G.T. Yee, J.M. Manriquez, D.A. Dixon, R.S. McLean, D.M. Groski, R.B. Flippen, K.S. Narayan, A.J. Epstein, and J.S. Miller, "Decamethylmanganocenium Tetracyanoethenide, $[Mn(C_5Me_5)_2]^{\bullet\bullet+}[TCNE]^{\bullet-}$–a Molecular Ferromagnet With an 8.8 K T_c," *Adv. Mater.*, **3** [6] 309-11 (1991).

[7] J.S. Miller, "Organometallic- and Organic-Based Magnets: New Chemistry and New Materials for the New Millennium," *Inorg. Chem.*, **39** [20] 4392-408 (2000).

[8] J.M. Manriquez, G.T. Yee, R.S. McLean, A.J. Epstein, and J.S. Miller, "A Room-Temperature Molecular/Organic-Based Magnet," *Science*, **252** 1415-17 (1991).

[9] K.I. Pokhodnya, D. Pejakovic, A.J. Epstein, and J.S. Miller, "Effect of Solvent on the Magnetic Properties of the High-Temperature $V[TCNE]_x$ Molecule-Based Magnet," *Phys. Rev. B*, **63** 174408 - 1-8 (2001).

[10] M.S. Thorum, K.I. Pokhodnya, and J.S. Miller, "Solvent Enhancement of the Magnetic Ordering Temperature (T_c) of the Room Temperature $V[TCNE]_x \cdot S$ (S = Solvent, TCNE = tetracyanoethylene; $x \sim 2$) Magnet," *Polyhedron*, **25** 1927-30 (2006).

[11] K.I. Pokhodnya, A.J. Epstein, and J.S. Miller, "Thin-Film $V[TCNE]_x$ Magnets," *Adv. Mater.*, **12** [6] 410-13 (2000).

[12] K.I. Pokhodnya, M. Bonner, and J.S. Miller, "Parylene Protection Coatings for Thin Film $V[TCNE]_x$ Room Temperature Magnets," *Chem. Mater.*, **16** [24] 5114-19 (2004).

[13] K.I. Pokhodnya, V. Burtman, A.J. Epstein, J.W. Raebiger, and J.S. Miller, "Control of Coercivity in Organic-Based Solid Solution $V_xCo_{1-x}[TCNE]_2 \cdot zCH_2Cl_2$ Room Temperature Magnets," *Adv. Mater.*, **15** [14] 1211-14 (2003).

[14] R.S. Edelstein, J. Yoo, N.P. Raju, J.D. Bergeson, K.I. Pokhodnya, J.S. Miller, and A.J. Epstein, "Organic-Based Magnetic Thin Films by Low Temperature CVD," *Mater. Res. Soc. Symp. Proc.*, **871E** 17.3.1-6 (2005).

[15] J.S. Miller, "Tetracyanoethylene (TCNE): The Characteristic Geometries and Vibrational Absorptions of Its Numerous Structures," *Angew. Chem. Int. Ed.*, **45** [16] 2508-25 (2006).

[16] Unpublished data of E. Shurda in the research lab of J.S. Miller.

[17] X. Liu, J.E. Ellis, T.D. Selby, P. Ghalsasi, and J.S. Miller, "Transition Metal Carbonyl Compounds. Hexacarbonylvanadate(1-) and Hexacarbonylvanadium(0)," *Inorg. Synth.*, **34** 96-103 (2004).

[18] G.S. Nolas, J. Sharp, and H.J. Goldsmid, *Thermoelectrics: Basic Principles and New Materials Development*, pp. 1-12, Springer-Verlag, Berlin Heidelberg, Germany, 2001.

[19] H.J. Goldsmid, *Thermoelectric Refrigeration*, pp. 202-9, Plenum Press, New York, 1964.

[20] *CRC Handbook of Chemistry and Physics*, 81st Ed., p. 12-119. Edited by D.R. Lide. CRC Press LLC, New York, 2000.